NAVAL POSTGRADUATE SCHOOL
Monterey, California

THESIS

COUPLED LAGRANGIAN AND EULERIAN APPROACH TO DETONATION AND FRAGMENTATION PROBLEMS

by

Mark S. Kloster

September 2001

Thesis Advisor: Young S. Shin

Approved for public release; distribution is unlimited

Report Documentation Page

Report Date	Report Type	Dates Covered (from... to)
30 Sep 2001	N/A	-

Title and Subtitle Coupled Lagrangian and Eulerian Approach to Detonation and Fragmentation Problems	**Contract Number**
	Grant Number
	Program Element Number
Author(s) Kloster, Mark	**Project Number**
	Task Number
	Work Unit Number
Performing Organization Name(s) and Address(es) Research Office Naval Postgraduate School Monterey, Ca 93943-5138	**Performing Organization Report Number**
Sponsoring/Monitoring Agency Name(s) and Address(es)	**Sponsor/Monitor's Acronym(s)**
	Sponsor/Monitor's Report Number(s)
Distribution/Availability Statement Approved for public release, distribution unlimited	
Supplementary Notes	
Abstract	
Subject Terms	
Report Classification unclassified	**Classification of this page** unclassified
Classification of Abstract unclassified	**Limitation of Abstract** UU
Number of Pages 82	

REPORT DOCUMENTATION PAGE			Form Approved OMB No. 0704-0188
Public reporting burden for this collection of information is estimated to average 1 hour per response, including the time for reviewing instruction, searching existing data sources, gathering and maintaining the data needed, and completing and reviewing the collection of information. Send comments regarding this burden estimate or any other aspect of this collection of information, including suggestions for reducing this burden, to Washington headquarters Services, Directorate for Information Operations and Reports, 1215 Jefferson Davis Highway, Suite 1204, Arlington, VA 22202-4302, and to the Office of Management and Budget, Paperwork Reduction Project (0704-0188) Washington DC 20503.			
1. AGENCY USE ONLY ***(Leave blank)***	**2. REPORT DATE** September 2001	**3. REPORT TYPE AND DATES COVERED** Master's Thesis	
4. TITLE AND SUBTITLE: Coupled Lagrangian and Eulerian Approach to Detonation and Fragmentation Problems			**5. FUNDING NUMBERS**
6. AUTHOR(S) Kloster, Mark			
7. PERFORMING ORGANIZATION NAME(S) AND ADDRESS(ES) Naval Postgraduate School Monterey, CA 93943-5000			**8. PERFORMING ORGANIZATION REPORT NUMBER**
9. SPONSORING / MONITORING AGENCY NAME(S) AND ADDRESS(ES) N/A			**10. SPONSORING / MONITORING AGENCY REPORT NUMBER**
11. SUPPLEMENTARY NOTES The views expressed in this thesis are those of the author and do not reflect the official policy or position of the Department of Defense or the U.S. Government.			
12a. DISTRIBUTION / AVAILABILITY STATEMENT Approved for public release; distribution is unlimited			**12b. DISTRIBUTION CODE**

13. ABSTRACT ***(maximum 200 words)***

Many obstacles such as minefields, barbwire entanglements, tank ditches and other fortifications are used to paralyze the forward momentum of mechanized armed forces. To combat this the Grizzly tracked vehicle was developed for the United States Army. Due to the Grizzly's mission various sensors, laser systems, hydraulic lines, wires and cameras are mounted on the armor hull, which are exposed to various types of landmine detonation and fragmentation. This thesis studies the effects of shock waves and fragmentation on the survivability of the equipment mounted on the Grizzly's armored hull. Models of an OZM-72 antipersonnel mine are developed and used to simulate the detonation and fragmentation phenomena. The analysis results obtained from the models provide a basis from which design guidance can be formulated for protecting equipment or personnel from this threat.

14. SUBJECT TERMS Detonation and Fragmentation Problems, Coupled Lagrangian and Eulerian Analysis, Antipersonnel Mines			**15. NUMBER OF PAGES** 67
			16. PRICE CODE
17. SECURITY CLASSIFICATION OF REPORT Unclassified	**18. SECURITY CLASSIFICATION OF THIS PAGE** Unclassified	**19. SECURITY CLASSIFICATION OF ABSTRACT** Unclassified	**20. LIMITATION OF ABSTRACT** UL

NSN 7540-01-280-5500 Standard Form 298 (Rev. 2-89)
Prescribed by ANSI Std. 239-18

THIS PAGE INTENTIONALLY LEFT BLANK

Approved for public release; distribution is unlimited

COUPLED LAGRANGIAN AND EULERIAN APPROACH TO DETONATION AND FRAGMENTATION PROBLEMS

Mark S. Kloster
Lieutenant, United States Navy
B.S., Norwich University, 1995

Submitted in partial fulfillment of the
requirements for the degree of

MASTER OF SCIENCE IN MECHANICAL ENGINEERING

from the

NAVAL POSTGRADUATE SCHOOL
September 2001

Author: _____
Mark S. Kloster

Approved by: _____
Young S. Shin, Thesis Advisor

_____
Terry R. McNelly, Chairman
Department of Mechanical Engineering

THIS PAGE INTENTIONALLY LEFT BLANK

ABSTRACT

Many obstacles such as minefields, barbwire entanglements, tank ditches and other fortifications are used to paralyze the forward momentum of mechanized armed forces. To combat this the Grizzly tracked vehicle was developed for the United States Army. Due to the Grizzly's mission various sensors; laser systems, hydraulic lines, wires and cameras are mounted on the armor hull, which are exposed to various types of landmine detonation and fragmentation. This thesis studies the effects of shock waves and fragmentation on the survivability of the equipment mounted on the Grizzly's armored hull. Models of an OZM-72 antipersonnel mine are developed and used to simulate the detonation and fragmentation phenomena. The analysis results obtained from the models provide a basis from which design guidance can be formulated for protecting equipment or personnel from this threat.

THIS PAGE INTENTIONALLY LEFT BLANK

TABLE OF CONTENTS

LIST OF FIGURES

LIST OF TABLES

THIS PAGE INTENTIONALLY LEFT BLANK

ACKNOWLEDGMENTS

I would like to extend my gratitude to Professor Young S. Shin for supporting me throughout my thesis. I greatly appreciate his scholarship and guidance. Thanks to COL Michael K. Asada and Mr. Brian Bonkosky at the United States Army Tank-automotive and Armaments Command (TACOM) for their support and problem identification, which made this thesis possible. I would also like to thank Tom Christian for his computer technical support and Chris Quan for his assistance with AUTODYN.

I dedicate this research to my parents who, through all life's endeavors, have inspired and supported me. To my wife Amiee, her comfort and encouragement has upheld me during my time at the Naval Postgraduate School.

THIS PAGE INTENTIONALLY LEFT BLANK

I. INTRODUCTION

A. BACKGROUND

1. Reason for Research

Landmines have posed a longstanding and serious threat to both personnel and vehicles of the armed forces. By using complex obstacles such as mine fields, barbwire entanglements, tank ditches and other fortifications an enemy can paralyze the forward movement of mechanized armed forces. Due to these threats the Grizzly Breach vehicle was designed for the United States Army [Ref. 8]. In order to perform its mission the

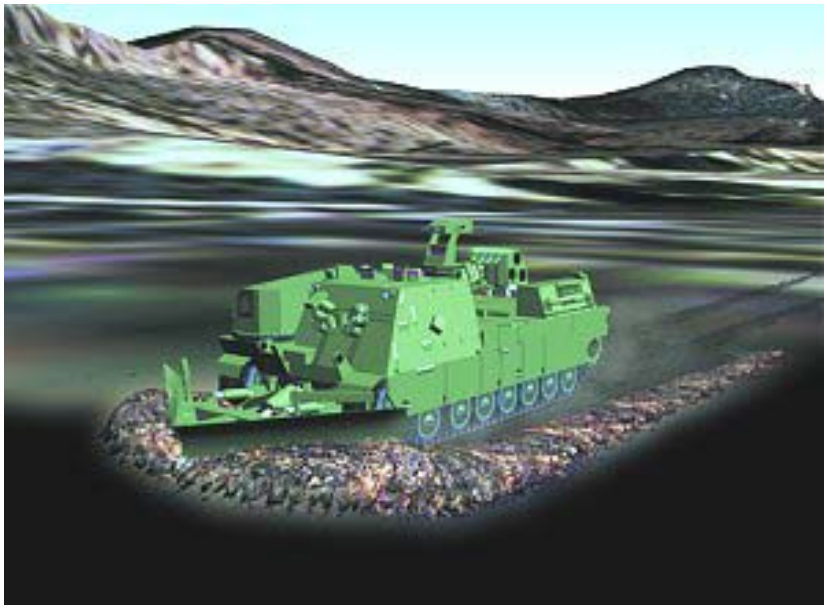

Figure 1. Grizzly Breach Vehicle [From Ref. 12]

Grizzly Breach Vehicle has various sensors, laser systems, hydraulic lines, wires and cameras mounted on its armored hull. Since they are out side the protective armor hull the various sensors and equipment are exposed and vulnerable to the detonation and fragmentation effects of bounding landmines. It is therefore important to understand the detonation and fragmentation phenomena of bounding landmines in order to provide guidance in the protection of equipment from this threat. Modeling and simulation of this phenomena is conducted using an OZM-72 bounding antipersonnel mine to provide insight into this phenomena.

2. Description of OZM-72 Antipersonnel Mine [Ref. 6]

a. General Description:

The OZM-72 antipersonnel mine is a cylindrical bounding fragmentation mine produced by the former Soviet Union. The casing of the mine is made of sheet steel, which contains steel wire fragments in a resin matrix. The top and bottom of the mine are steel plates with the detonator centrally located on the top plate.

b. Method of Operation:

The mine operates by first igniting a propelling charge, which lifts the fragmentation portion of the mine off the ground. Once the mine has reached a height of approximately 1.0 meter an anchor wire initiates the detonation of the main charge. The main charge detonation propels the steel fragments out to a claimed lethal radius of 25 meters.

c. Technical Specifications:

Height = 160 mm

Diameter = 105 mm

Total Weight = 5 kg

Explosive Weight = 500 g TNT

Fragment Dimensions:
Length = 5mm Diameter = 5mm

Table 1. OZM-72 Technical Data

Figure 2. OZM-72 Landmine [From Ref. 5]

B. SCOPE OF REASEARCH

This paper investigates the detonation and fragmentation phenomena of bounding antipersonnel mines. This is undertaken to provide a better understanding of the fragmentation threat posed by this type of weapon. To accomplish this a coupled Lagrangian and Eulerian approach was used in modeling this phenomena. Two-dimensional and three-dimensional models where created of the OZM-72 antipersonnel mine using the AUTODYN interactive nonlinear dynamics analysis software. These models were used in providing insight into the detonation and fragmentation phenomena. The analysis results obtained from the models provide a basis from which design guidance can be formulated for protecting equipment or personnel from this threat.

THIS PAGE INTENTIONALLY LEFT BLANK

II. AUTODYN COMPUTATIONAL SETUP

A. SOLUTION TECHNIQUE

AUTODYN solves complex dynamic behavior problem by discretization of the problem in both time and space. Time is broken into time steps, which are determined by the software to maintain accuracy and stability of the solution. Space is divided into elements, which are six sided bricks that are organized by a structured IJK index grid.

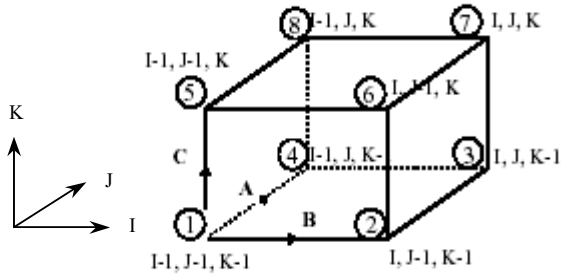

Figure 3. IJK Brick Element [From Ref. 4]

Within each problem several IJK index grids (sub grids) can be used allowing for complex shapes to be described or coupling of different processor types.

B. PROCESSOR TYPE

AUTODYN has several processor types available, which can be used in a given problem to provide the optimal numerical solution for the given problem. The processors used in this study are the Lagrange and the Euler-FCT.

1. Lagrange

The Lagrange processors algorithms are based on the finite volume method used by Wilkins in the HEMP code. This formulation has been modified slightly in order to accommodate forces and masses at the nodes similar to explicit finite element formulations. This modification enabled a simpler coupling between Lagrange and Euler processors [Ref. 4]. The Lagrange processor solves problems by replacing the partial differential equations for conservation of mass, momentum and energy with finite difference equations solved using an explicit central difference scheme.

The numerical mesh in of the Lagrange processor moves with the materials defined in the sub grid. Meaning that no material is transported between elements through the element faces. Properties for each element are defined either at the node corners or at the cells center, as shown in the figure below.

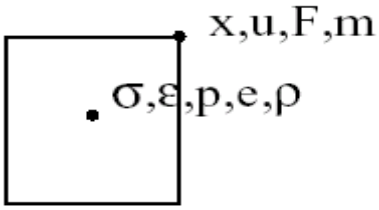

Figure 4. Element Property Locations [From Ref. 3]

Where x is the coordinate, u is the velocity, F is the force, m is the mass, σ is the stress, ε is the strain, p is the pressure, e is the internal energy, and ρ is the density.

a. Computational Cycle

The steps the Lagrange processor conducts for each time step in a Lagrangian sub grid are shown in the following diagram.

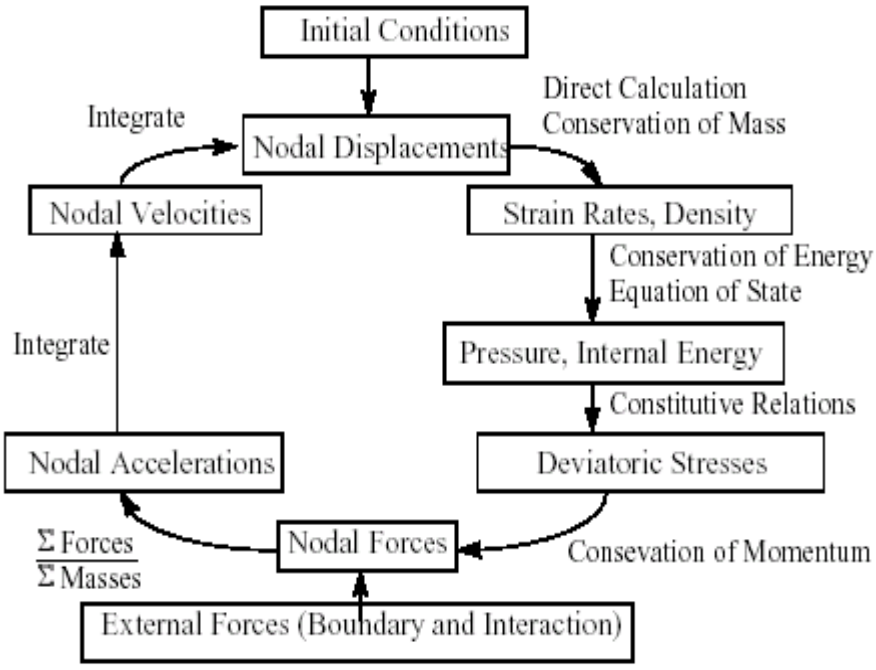

Figure 5. Lagrange Computational Cycle [From Ref. 3]

Since the algorithm used is an explicit scheme each time step for Lagrangian sub grids must satisfy the CLF or Conart condition

$$\Delta t < \frac{\Delta x}{c} \tag{2.1}$$

were Δx is the element size and c is the local speed of sound. The minimum value for the sub grid is then multiplied by a safety factor of two-thirds and is used to advance the solution in time. The reason for this restriction is to ensure a disturbance dose not propagate across an element in a single time step and to maintain stability of the algorithm.

b. Advantages

The advantages of using the Lagrange processor in modeling are as follows:

- Computations per cycle are fewer than that of a Eulerian processor.
- Material boundaries and interfaces are clearly defined and do not mix.
- Well suited for modeling solid behavior and strength.

c. Disadvantages

The disadvantages of using the Lagrange processor in modeling are as follows:

- Sever element distortions lead to small time steps.
- Element distortions can lead to grid tangling causing the simulation to stop.

These disadvantages can be overcome by the use of the erosion feature provided in AUTODYN.

2. Euler – FCT

The Euler – FCT processor is designed specifically to solve gas dynamics problems and in particular blast simulations. FCT stands for Flux Corrected Transport. The algorithm is a multi-dimensional implementation of the explicit FCT formulation of

Boris and Book [Ref. 4]. Like in the Lagrange processor, the Euler processor solves problems by replacing the partial differential equations for conservation of mass, momentum and energy with finite difference equations solved using an explicit central difference scheme.

Unlike the Lagrange processor, the Eulerian numerical grid is fixed allowing materials to flow through the element faces from one element to another. Properties for each element are defined either at the node corners or at the cells center, as shown in the figure below.

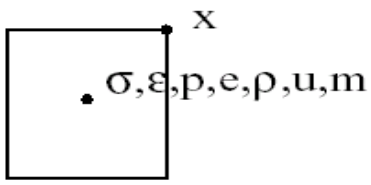

Figure 6. Element Property Locations [From Ref. 3]

Where x is the displacement, u is the velocity, F is the force, m is the mass, σ is the stress, ε is the strain, p is the pressure, e is the internal energy, and ρ is the density.

a. Computational Cycle

The steps the Euler processor conducts for each time step in a Eulerian sub grid are shown in the following diagram.

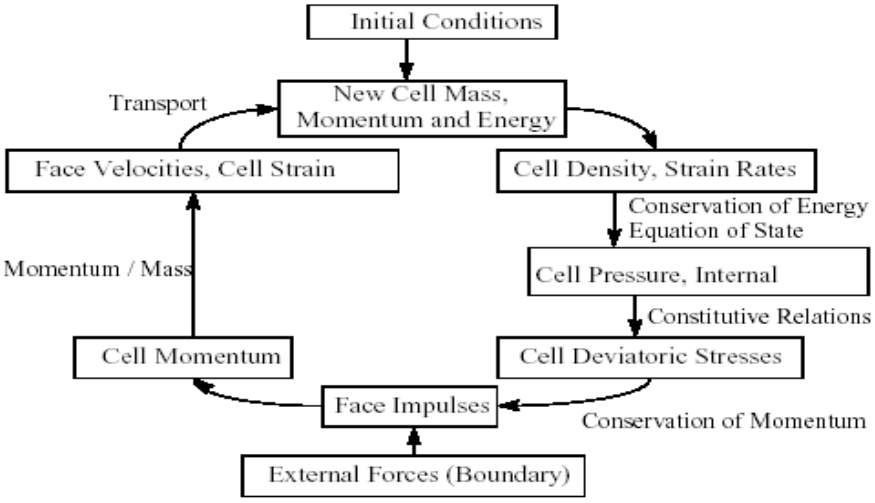

Figure 7. Eulerian Computational Cycle [From Ref. 3]

Since the algorithm used is an explicit scheme each time step for Eulerian sub grids must satisfy the CLF or Conart condition

$$\Delta t < \frac{\Delta x}{\left(c + |v|\right)} \tag{2.2}$$

were Δx is the element size, c is the local speed of sound, and v is the element velocity. The minimum value for the sub grid is then multiplied by a safety factor of two-thirds and is used to advance the solution in time. The reason for this restriction is to ensure a disturbance dose not propagate across an element in a single time step and to maintain stability of the algorithm.

b. Advantages

The advantages of using the Euler-FCT processor in modeling are as follows:

- No grid distortions or tangling reducing time step or stopping the simulation.
- Accurate higher order method optimized for blast type problems.

c. Disadvantages

The disadvantages of using the Euler-FCT processor in modeling are as follows:

- More computations per cycle are required than that of a Lagrange processor.
- Only allowed to place one material in each sub grid.
- Only allowed to use the ideal gas equation of state to define the material in the sub grid.

C. MATERIAL MODELS

The material models in AUTODYN can be broken down into three categories. These categories are the equation of state, which is used in providing volumetric stress or pressure. The strength models, which are the constitutive relations for determining the

deviatoric stresses by Hooke's Law and a plastic yield criteria. The last is the failure model, which provides a criterion for determining if a material has failed and no longer has strength.

1. Equations of State

a. Ideal Gas

The ideal gas equation of state relates the pressure (p) to the specific internal energy (e), such that

$$p = (\gamma - 1)\rho \mathrm{e} \tag{2.3}$$

where γ is the adiabatic constant (ratio of specific heats) and ρ is the density.

b. JWL

The JWL equation of state defines the explosive shock wave pressure (p) as a function of the specific volume (V) and the specific internal energy (e), such that

$$p = C_1\left(1 - \frac{\omega}{r_1 V}\right)e^{-r_1 V} + C_2\left(1 - \frac{\omega}{r_2 V}\right)e^{-r_2 V} + \frac{\omega \mathrm{e}}{V} \tag{2.4}$$

where variables ω, C_1, C_2, r_1, and r_2 are constants for a specific explosive. These constants are determined from data collected during cylinder test.

c. Linear

The linear equation of state considers pressure (p) a function of density (ρ) by an approximation to Hook's Law, such that

$$p = K\mu \tag{2.5}$$

where $\mu = \left(\rho / \rho_0\right) - 1$ the compression, ρ_o is the reference density, and K is the materials bulk modulus.

2. Strength Models

The main purpose of the strength models is to determine when a material should yield. In AUTODYN all the strength models use the Von Mises yield criterion to determine the elastic limit and the onset of plastic flow. The Von Mises yield criteria

states that the deviatoric stresses (distortion) s_1, s_2, and s_3 are related to the yield strength (Y) by

$$s_1^{\,2} + s_2^{\,2} + s_3^{\,2} = \frac{2Y^2}{3} \tag{2. 6}$$

meaning the onset of yielding is purely a function of the distortion of the material and does not depend on the local hydrostatic pressure unless the yield strength is a function of pressure.

a. Von Mises Model

The Von Mises model is the simplest and most convenient criteria to describe the elastic limit and the transition to plastic flow. This model defines the yield stress (Y) as a constant, which is entered by the user.

3. Failure Model

a. Bulk Strain

This simple model states that bulk failure of a material element will occur when the effective plastic strain exceeds a specified value. Once this limit is reached the stress deviators are set to zero and the element material can no longer sustain any shear strength.

4. Erosion Model

During simulations some Lagrangian element can become severely distorted which can slow the progress of the calculations. In AUTODYN these cells can be removed from the calculation if a predetermined strain exceeds a user specified limit.

D. PROCESSOR COUPLING

Due to AUTODYN's coupling ability, separate numerical sub grids with the same or different types of processors can be used to describe a given problem. This allows for the use of the best type of processor to be used in modeling the problem. Since the interactions of the sub grids are also need to be calculated the following is a diagram of the complete computational cycle.

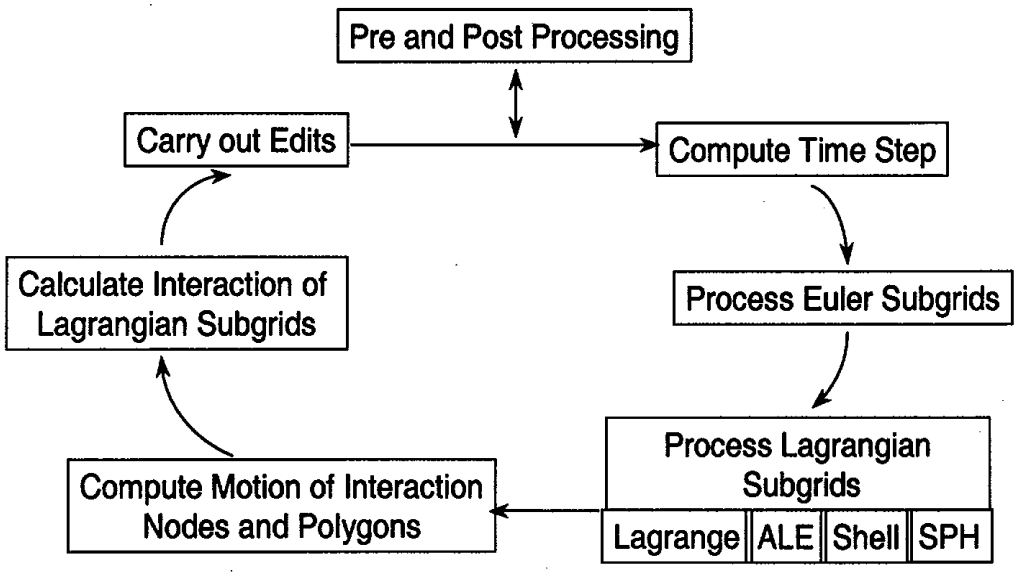

Figure 8. Complete Computational Cycle [From Ref. 7]

For this study the types of processor coupling that were used are the joined Lagrange, impact/slide interface and the Euler-Lagrange coupling.

1. Joined Lagrange

For the joined Lagrange type of processor coupling the connected nodes of Lagrangian sub grids are fused together and are regarded as a single node in the calculations. Meaning the joined nodes will remain together unless the joined condition is removed or element erosion occurs.

2. Impact/Slide Interface

Impact/Slide interface is used in determining the interactions between Lagrangian sub grids which impact or slide along each other. This interaction algorithm is based on the use of a small gap to determine if sub grids are interacting. This gap defines a zone around each interacting face that is used in determining if the sub grids will collide during a time step. To determine if sub grids interact an array of the current surface faces of one sub grid is comparing to the surface nodes of another sub grid. If any of the surface nodes enter the other grids gap zone, momentum-conserving interactions are computed to prevent the penetration of the sub grids. This procedure is repeated by exchanging the sub grids in order to provide symmetry to the process [Ref. 3]

3. Euler – Lagrange Coupling

The Eulerian and Lagrangian sub grids are coupled by using an algorithm, which defines a stress profile for the Lagrangian sub grid. The stress profile is based on the geometric flow constraint placed on the Eulerian sub grid as the Lagrangian grid passed through it. While Lagrangian sub grid moves and distorts through the Eulerian sub grid elements are covered and uncovered. Due to this fact a sophisticated logic is used to avoid the Eulerian elements from becoming to small. This is done in order to ensure the time step is not severely reduced. With this type of coupling algorithm complex fluid-structure interaction problems can be solved using the best processor for the job.

E. REMAPPING

Remapping is a method by which a user is able to take the solution of one analysis and impose it upon all regions of a selected region of a different model. This is accomplished by creating a remap data fill, which contains the data of the analysis that is to be remapped. The file is then loaded into the receptor sub grid, which provides the receptor sub grid with the data from the previous solution.

THIS PAGE INTENTIONALLY LEFT BLANK

III. VULNERABILITY ASSESSMENT

A. DAMAGE MECHANISM

For bounding antipersonnel mines the damage is created by the detonation and fragmentation phenomena. In these phenomena the energy of an explosive shock wave is transferred to the fragmentation material, which is used to damage a target. For antipersonnel mines the explosive shock wave is produced by the rapid energy release of an explosive charge. The shock wave produced by this energy release travels faster than the speed of sound, has a limited duration and possesses a significant amount of energy. The energy contained within the shock wave is then transferred to the fragmenting material in the form of kinetic energy. The kinetic energy of the fragmenting material is the mechanism by which damage is caused to targets. The kinetic energy of a fragment is found by the equation:

$$KE = \frac{1}{2} mv^2 \tag{3.1}$$

where m is the mass of the fragment and v is the velocity of the fragment. Since the fragments travel thru the air the velocity of the fragments will decrease due to the drag created by the air. The velocity of a fragment at a specified distance can be determined by the equation [Ref. 11]

$$v_s = v_0 e^{\frac{-\rho C_d A S}{2m}} \tag{3.2}$$

where v_o is the initial velocity, ρ is the density of the fluid, C_d is the drag coefficient of the fragment, A is the cross-sectional area of the fragment, S is the distance, and m is the mass of the fragment.

B. PROBABILITY OF KILL

The probability of kill (P_k) is a statistical measure of a targets ability to withstand the damage caused by one or more damage mechanisms. Probability of kill is a function of whether a damage mechanism reaches a target and the likelihood the target will be destroyed or killed by the damage mechanism. In this study the probability of kill was determined based on the damage mechanism described in section A of this chapter.

For antipersonnel mines the probability of kill is determined by finding the number of fragments that impact a target and the probability of kill per fragment ($P_{k/f}$). From these values a probability of kill is determined by the use of the following equations [Ref. 2 and 11]

$$P_k = 1 - \left(1 - P_{k/f}\right)^{N_t} \qquad \text{For: N > 1} \qquad (3.3)$$

$$P_k = N_t \left(P_{k/f}\right) \qquad \text{For: 0 < N < 1} \qquad (3.4)$$

where N_t is the number of fragments impacting the target.

For this study the probability of kill is determined by finding the average kinetic energy of the fragments from the average velocity of the fragments. From this the probability of kill per fragment was determined by linear interpolation of Table 2.

	Kinetic Energy (Joules)		
Target	$P_{k/f} = 0.1$	$P_{k/f} = 0.5$	$P_{k/f} = 0.9$
Soft	100	1000	4000
Hard	4000	10000	20000

Table 2. Probability of Kill Per Fragment [After Ref. 11]

Where soft targets can be considered to be personnel or fragile sensors and hard targets can be considered to be body armor or light metals like aluminum.

The number of fragments impacting a target is determined by considering an ideal case. In this case the mine is considered to be level, the spray pattern of the fragments is cylindrical with the fragments only traveling in the radial direction. The targets are considered to be in the direct path of the fragments and have a height equal to that of the mine. The following equation is used to determine the number of fragments impacting the target

$$N_t = w\left(\frac{N_m}{2\pi R}\right) \qquad (3.5)$$

where w is the width of the target, N_m is the number of fragments in the mine, and R is the distance the target is from the mine.

IV. MINE EXPLOSION MODELS

A. EXPLOSIVE MODEL

The explosive for the mine models was modeled separately from the remainder of the mine. The results produced by the explosive model were placed into the two-dimensional and three-dimensional mine models using the remap feature available in AUTODYN. This was accomplished in order to reduce the computation time for the model and so that the shock wave pressure could be modeled using the JWL equation of state.

The explosive model is composed of a single sub grid, which used the Eulerian processor and was filled with a material model that has a JWL equation of state. The material model input deck can be found in Appendix A. The sub grid is composed of a square that is 67mm in the x direction and 27mm in the y direction with an I index of 68 and a J index of 28 (1876 elements). In addition, an axial symmetry boundary and a detonation boundary were placed along the x-axis. Figure 9 is a depiction of the TNT sub grid.

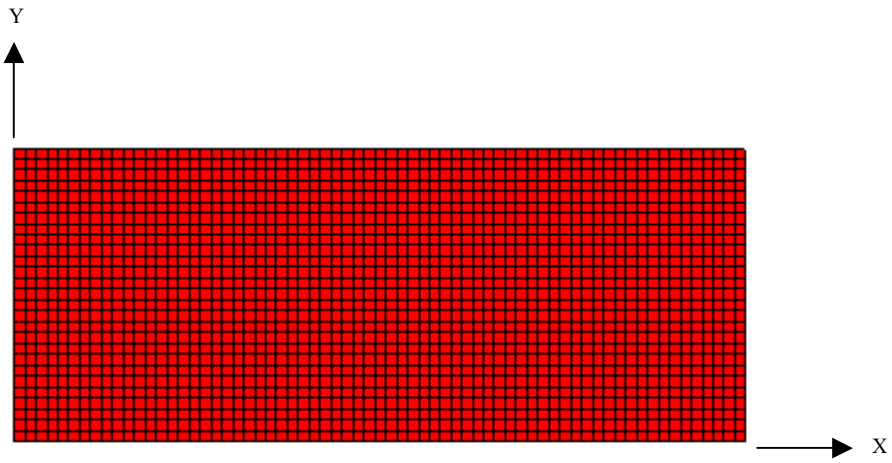

Figure 9. Explosive Model

The dimensions of the TNT sub grid were chosen in order to provide the appropriate mass of explosive to the models.

B. TWO-DIMENTIONAL MINE MODELS

The two-dimensional mine models were developed based on a quarter of a slice of the mine when viewed from the top or bottom of the mine. Each of these models contains three sub grids and has symmetry boundaries along the x, y and z-axis.

1. Four-Row Mine Model

Figure 10 is a depiction of the assembled four-row mine model.

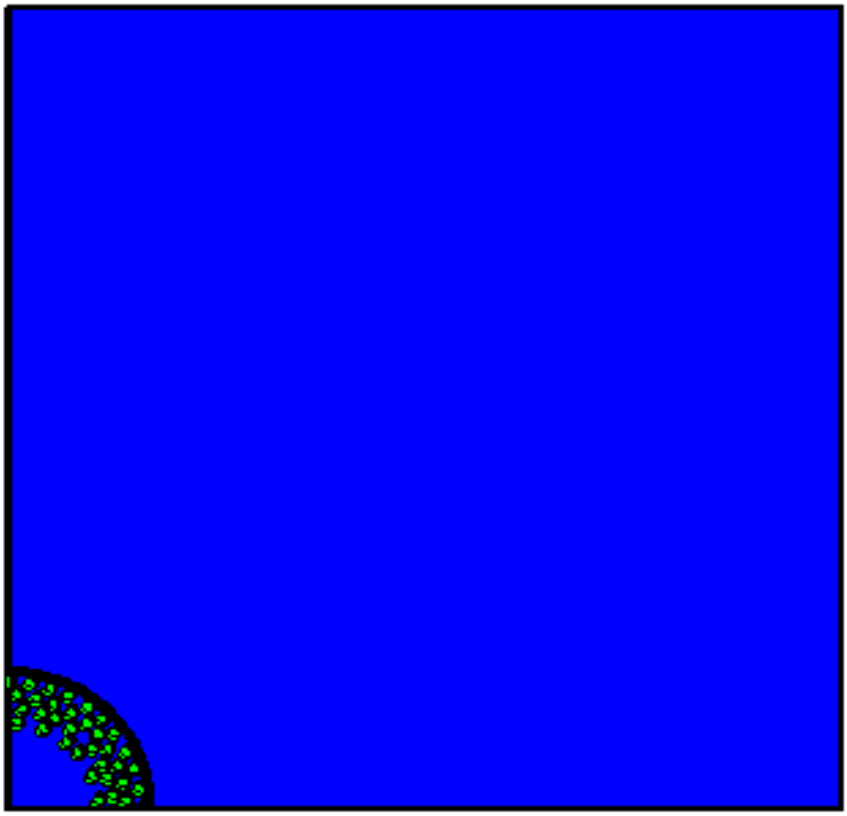

Figure 10. Four-Row Mine Model

In Figure 10 the blue portion is the air sub grid, the gray is the shell sub grid and the green is the wire sub grid.

a. Air Sub Grid

The air sub grid used the Euler-FCT processor and was filled with a material model, which used the ideal gas equation of state. The material input deck can be found in Appendix B. The sub grid is composed of a block that is 5mm in the x

direction and 300mm in both the y and z directions with an I index of 6, and a J and K index of 101 (50000 elements). In addition non-reflecting boundaries were placed along the faces indicated in Figure 11.

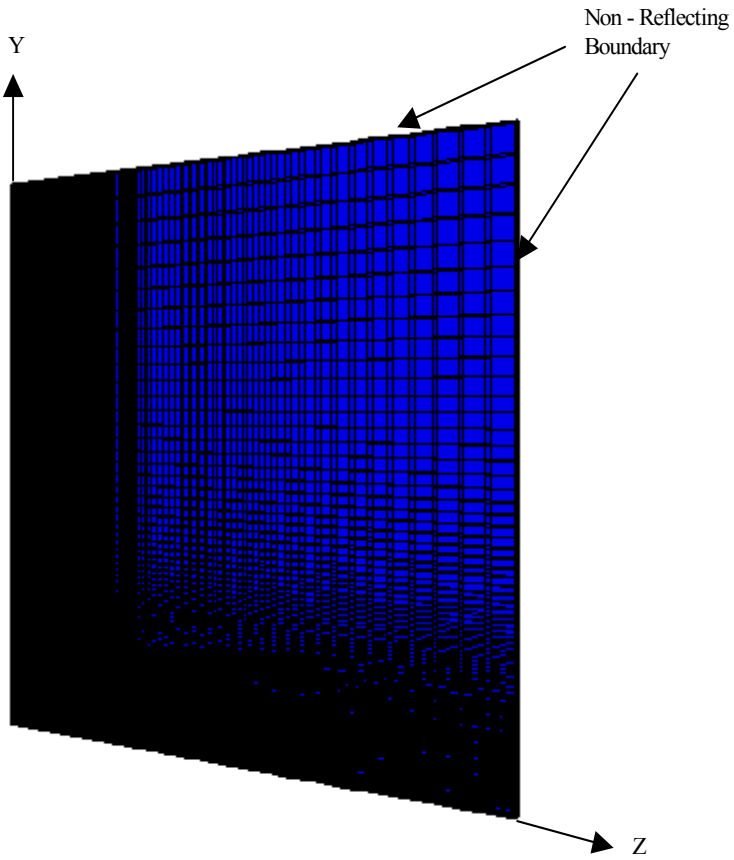

Figure 11. Four-Row Model of the Air Sub Grid

The explosive shock wave produce by the explosive model was remapped into the air sub grid after the sub grid was produced.

b. Wire Sub Grid

The wire sub grid used the Lagrange processor and was filled with a material model, which used the linear equation of state. The material input deck can be found in Appendix C. The sub grid is composed of 34 cylinders each having a diameter of 5mm, a length of 5mm and arranged as shown in Figure 12. Each of the cylinders has an I and J index of 5 and a K index of 4 (48 elements).

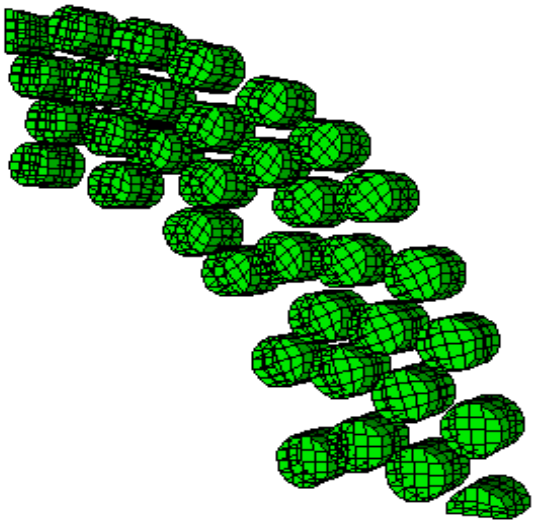

Figure 12. Four-Row Model of the Wire Sub Grid

c. Shell Sub Grid

The shell sub grid used the Lagrange processor and was filled with a material model, which used the linear equation of state, the Von Mises strength model, the bulk strain failure model and the erosion model. The material input deck can be found in Appendix D. The sub grid is composed of ¼ of a hollow cylinder with an inner radius of 50mm, an outer radius of 52mm and a length of 5mm with a I index of 2, a J index of 51, and a K index of 4 (153 elements). Figure 13 is a depiction of the shell sub grid.

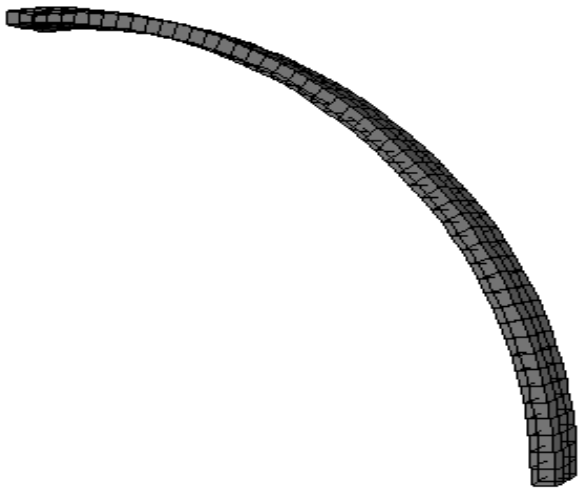

Figure 13. Four-Row Model of the Shell Sub Grid

2. Three-Row Mine Model

Figure 14 is a depiction of the assembled three-row mine model.

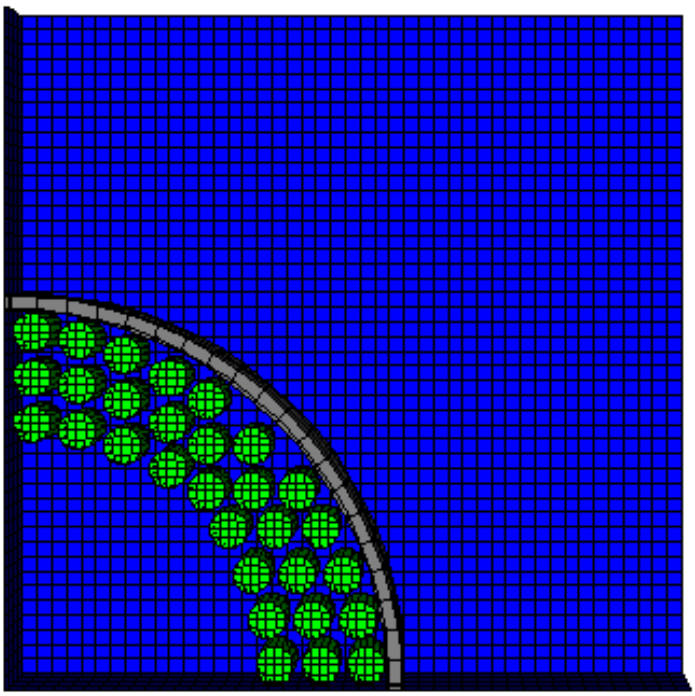

Figure 14. Three-Row Mine Model

In Figure 14 the blue portion is the air sub grid, the gray is the shell sub grid and the green is the wire sub grid.

a. Air Sub Grid

The air sub grid used the Euler-FCT processor and was filled with a material model, which used the ideal gas equation of state. The material input deck can be found in Appendix B. The sub grid is composed of a block that is 5mm in the x direction and 90mm in both the y and z directions with an I index of 5 and a J and K index of 46 (8100 elements). In addition non-reflecting boundaries were placed along the faces indicated in Figure 15.

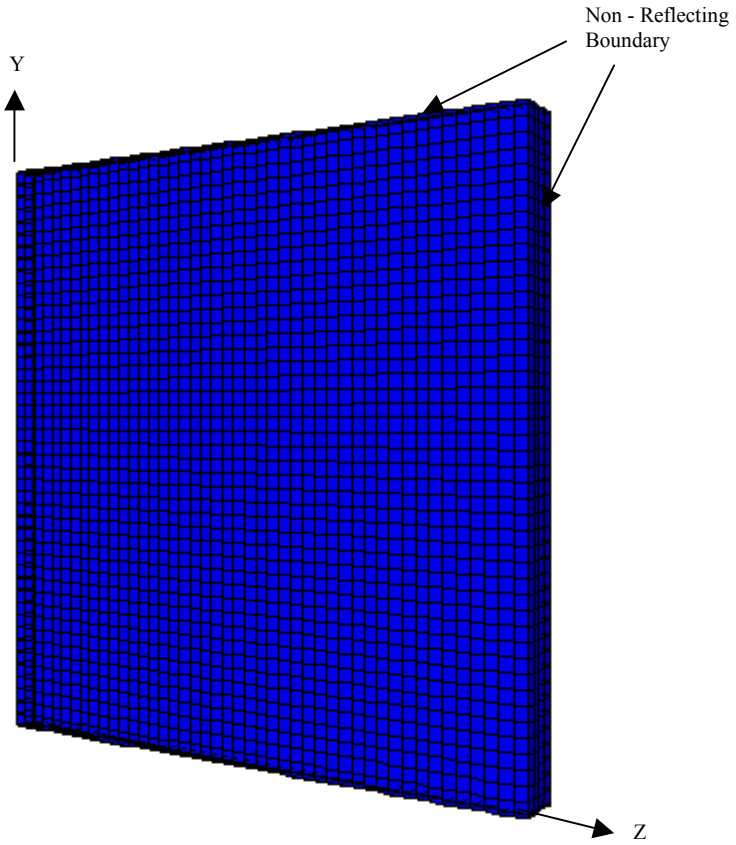

Figure 15. Three-Row Model of the Air Sub Grid

The explosive shock wave produce by the explosive model was remapped into the air sub grid after the sub grid was produced.

b. Wire Sub Grid

The wire sub grid used the Lagrange processor and was filled with a material model, which used the linear equation of state. The material input deck can be found in Appendix C. The sub grid is composed of 30 cylinders each having a diameter of 5mm, a length of 5mm and arranged as shown in Figure 16. Each of the cylinders has an I and J index of 5 and a K index of 2 (16 elements).

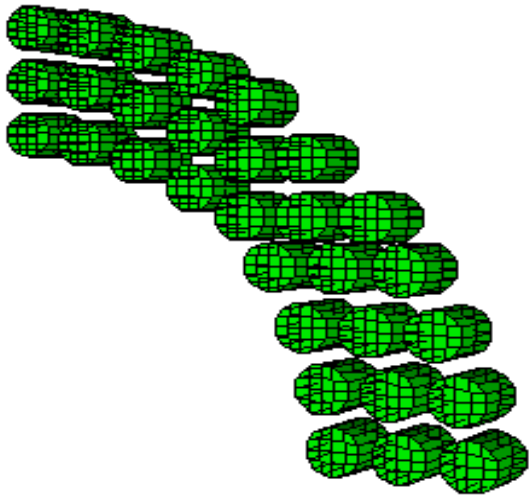

Figure 16. Three-Row Model of the Wire Sub Grid

c. Shell Sub Grid

The shell sub grid used the Lagrange processor and was filled with a material model, which used the linear equation of state, the Von Mises strength model, the bulk strain failure model and the erosion model. The material input deck can be found in Appendix D. The sub grid is composed of ¼ of a hollow cylinder with an inner radius of 50mm, an outer radius of 52mm and a length of 5mm with a I index of 2, a J index of 21, and a K index of 4 (60 elements). Figure 17 is a depiction of the shell sub grid.

Figure 17. Three-Row Model of the Shell Sub Grid

3. Two-Row Mine Model

Figure 18 is a depiction of the assembled two-row mine model.

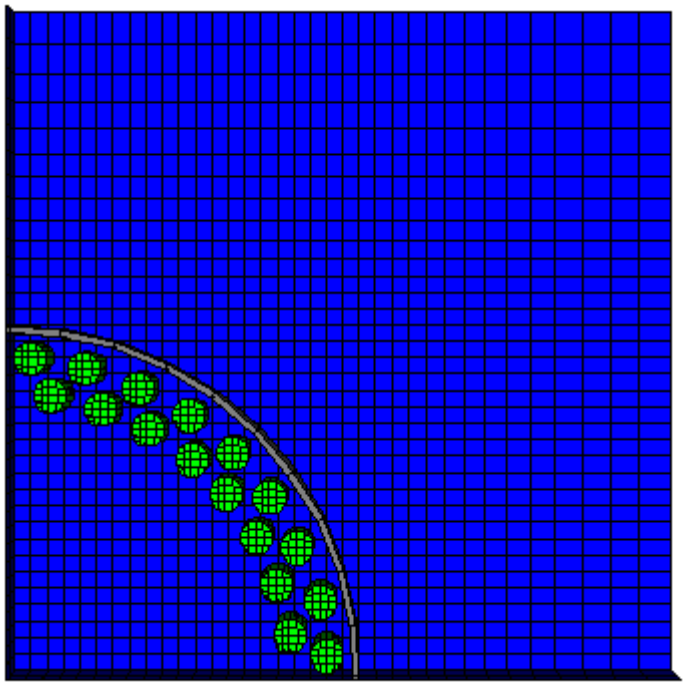

Figure 18. Two-Row Mine Model

In Figure 18 the blue portion is the air sub grid, the gray is the shell sub grid and the green is the wire sub grid.

a. Air Sub Grid

The air sub grid used the Euler-FCT processor and was filled with a material model, which used the ideal gas equation of state. The material input deck can be found in Appendix B. The sub grid is composed of a block that is 5mm in the x direction and 100mm in both the y and z directions with an I index of 3 and a J and K index of 36 (2450 elements). In addition non-reflecting boundaries were placed along the faces indicated in Figure 19.

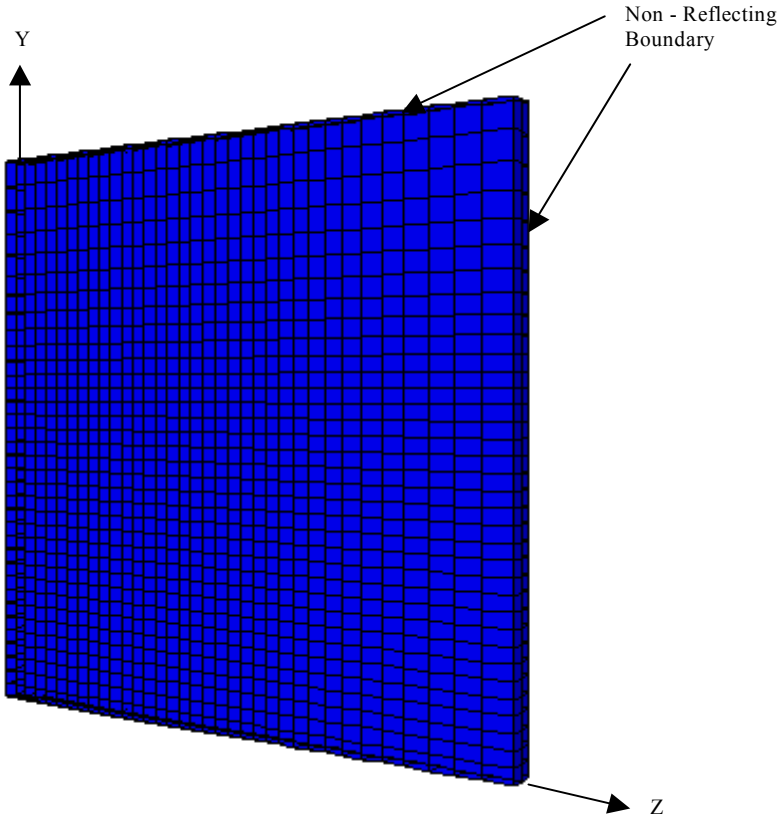

Figure 19. Two-Row Model of the Air Sub Grid

The explosive shock wave produce by the explosive model was remapped into the air sub grid after the sub grid was produced.

b. Wire Sub Grid

The wire sub grid used the Lagrange processor and was filled with a material model, which used the linear equation of state. The material input deck can be found in Appendix C. The sub grid is composed of 17 cylinders each having a diameter of 5mm, a length of 5mm and arranged as shown in Figure 20. Each of the cylinders has an I and J index of 5 and a K index of 2 (16 elements).

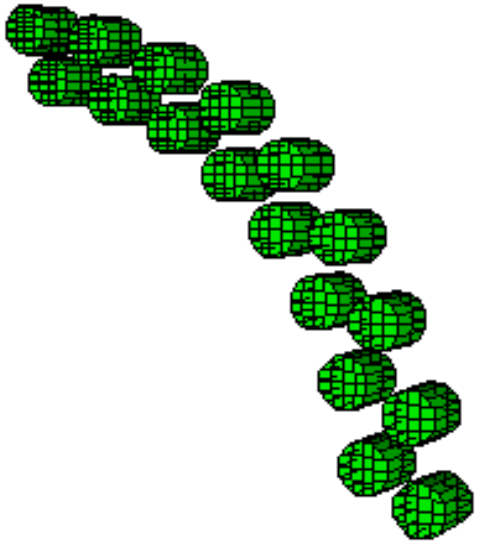

Figure 20. Two-Row Model of the Wire Sub Grid

c. Shell Sub Grid

The shell sub grid used the Lagrange processor and was filled with a material model, which used the linear equation of state, the Von Mises strength model, the bulk strain failure model and the erosion model. The material input deck can be found in Appendix D. The sub grid is composed of ¼ of a hollow cylinder with an inner radius of 51.5mm, an outer radius of 52.5mm and a length of 5mm with a I index of 2, a J index of 11 and a K index of 2 (10 elements). Figure 21 is a depiction of the shell sub grid.

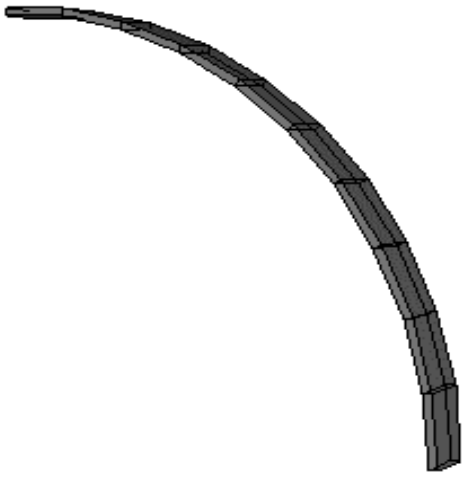

Figure 21. Four-Row Model of the Shell Sub Grid

C. THREE-DIMENTIONAL MINE MODEL

The three-dimensional mine model was developed based on one eighth of the mine and had a wire sub grid similar to that of the two row mine model. Unlike the two-dimensional mine models the three-dimensional mine model has an additional sub grid which models the top or bottom of the mine. Like the two-dimensional models symmetry boundaries were created along the x, y, and z-axis. Figure 22 is a depiction of the assembled three-dimensional mine model.

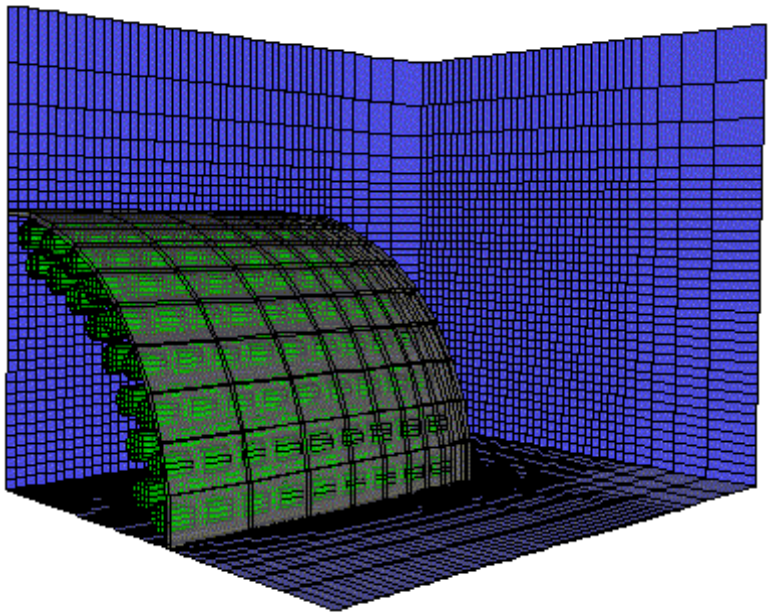

Figure 22. Three-Dimensional Mine Model

1. Air Sub Grid

The air sub grid used the Euler-FCT processor and was filled with a material model, which used the ideal gas equation of state. The material input deck can be found in Appendix B. The sub grid is composed of a block that is 110mm in the x direction and 90mm in both the y and z directions with an I index of 46 and a J and K index of 36 (55125 elements). In addition non-reflecting boundaries were placed along the block faces indicated in Figure 23.

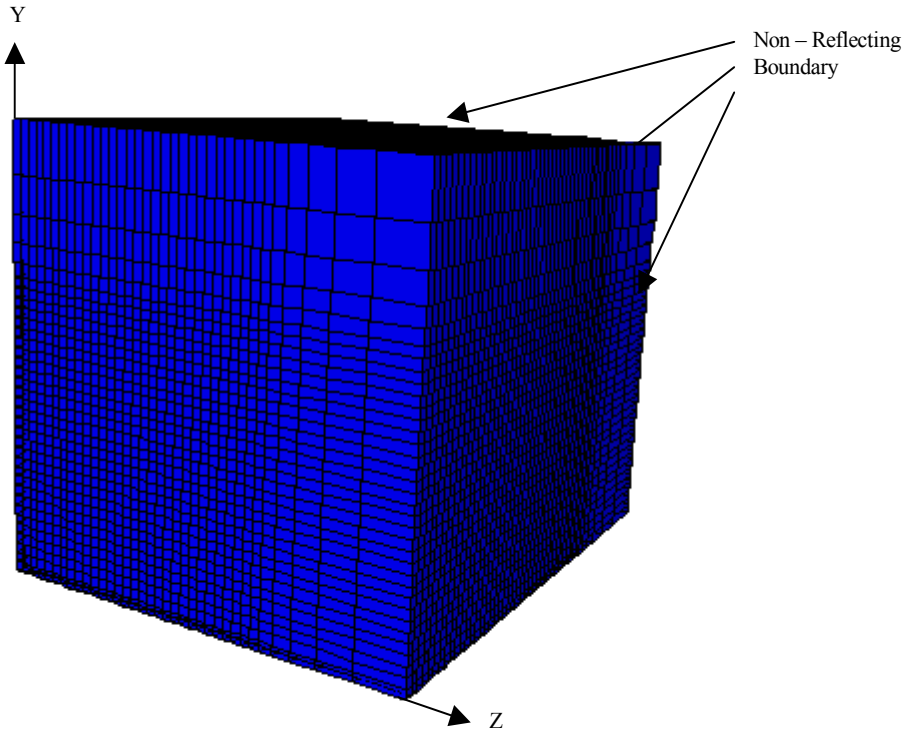

Figure 23. Three-Dimensional Model of the Air Sub Grid

The explosive shock wave produce by the explosive model was remapped into the air sub grid after the sub grid was produced.

2. Wire Sub Grid

The wire sub grid used the Lagrange processor and was filled with a material model, which used the linear equation of state. The material input deck can be found in Appendix C. The sub grid is composed of 153 cylinders each having a diameter of 5mm, a length of 5mm and arranged as shown in Figure 24. Each of the cylinders has an I and J index of 5 and a K index of 2 (16 elements).

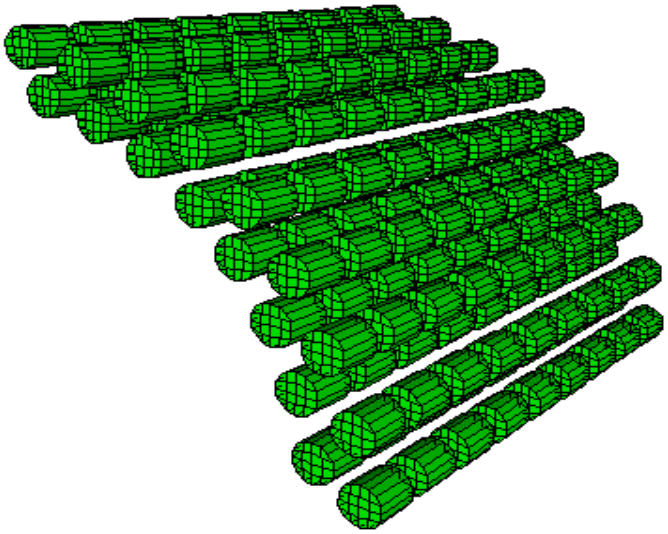

Figure 24. Three-Dimensional Model of the Wire Sub Grid

3. Shell Sub Grid

The shell sub grid used the Lagrange processor and was filled with a material model, which used the linear equation of state, the Von Mises strength model, the bulk strain failure model and the erosion model. The material input deck can be found in Appendix D. The sub grid is composed of ¼ of a hollow cylinder with an inner radius of 51.5mm, an outer radius of 52.5mm and a length of 70mm with a I index of 2 and a J and K index of 11 (100 elements). Figure 25 is a depiction of the shell sub grid.

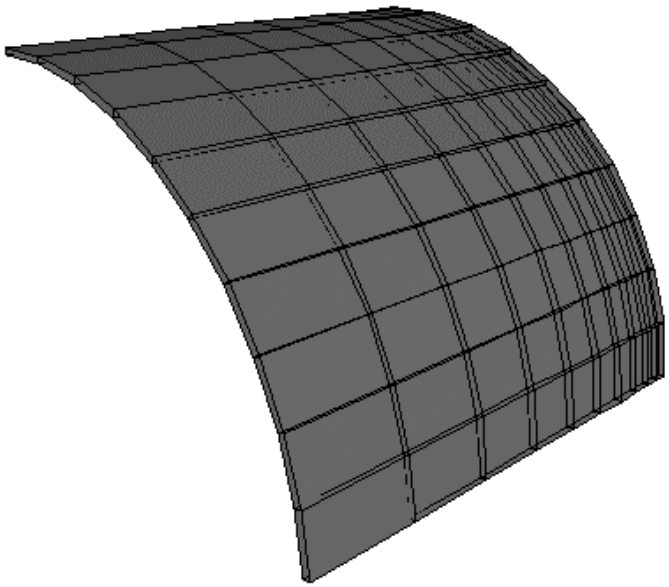

Figure 25. Three-Dimensional Model of the Shell Sub Grid

4. Cap Sub Grid

The cap sub grid used the Lagrange processor and was filled with a material model, which used the linear equation of state, the Von Mises strength model, the bulk strain failure model and the erosion model. The material input deck can be found in Appendix D. The sub grid is composed of ¼ of a solid cylinder with an outer radius of 51.5mm and a length of 2mm with an I and J index of 11 and a K index of 2 (75 elements). Figure 26 is a depiction of the cap sub grid.

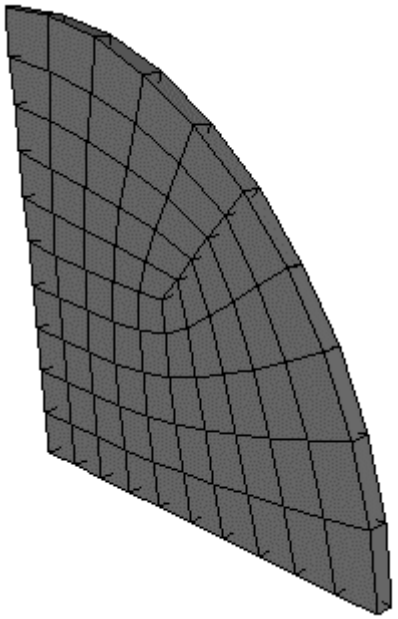

Figure 26. Three-Dimensional Model of the Shell Sub Grid

The cap sub grid was joined to the shell sub grid using the joined Lagrange processor coupling. This was done in order to have a rigid connection between the steel sheet casing and the top plate of the mine.

V. ANALYSIS RESULTS

All of the analysis results for this thesis were obtained using a Dell Dimension XPS T800r computer with an 800 MHz Intel Pentium Three processor and 640 mega bites of RAM.

A. FOUR-ROW MINE MODEL

The simulation of the four-row mine model required a run time of approximately 75 hours and 36 minutes and a total of 10000 time steps were computed, with a final cycle time of 0.159ms.

After 0.074ms (2900 cycles) the shell sub grid and the wire sub grid have expanded in the radial direction with the shell sub grid starting to break apart as shown in Figure 27. With Figure 28 showing the wire and shell sub grids velocities for the same cycle.

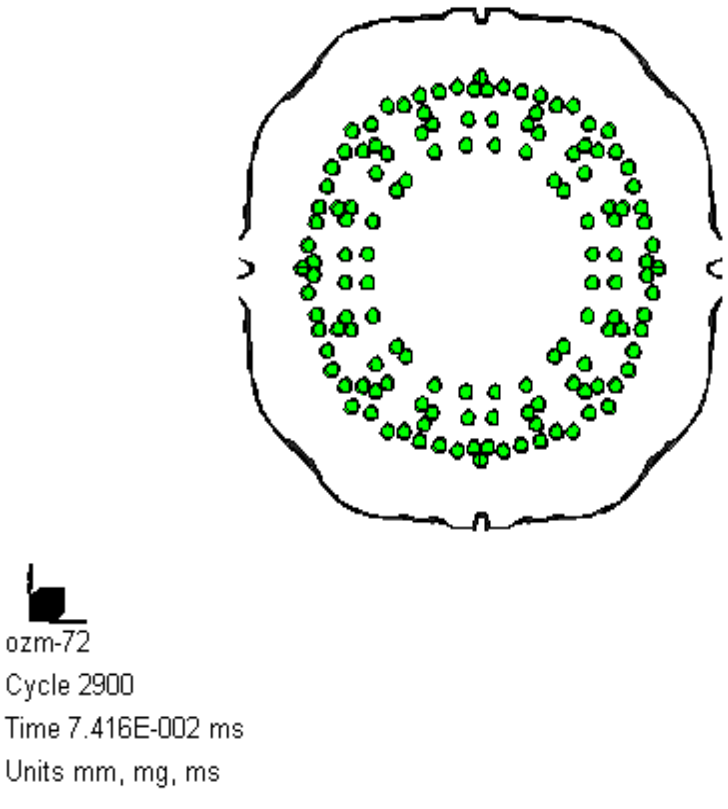

Figure 27. Expansion of the Four-Row Mine Model at 0.074ms

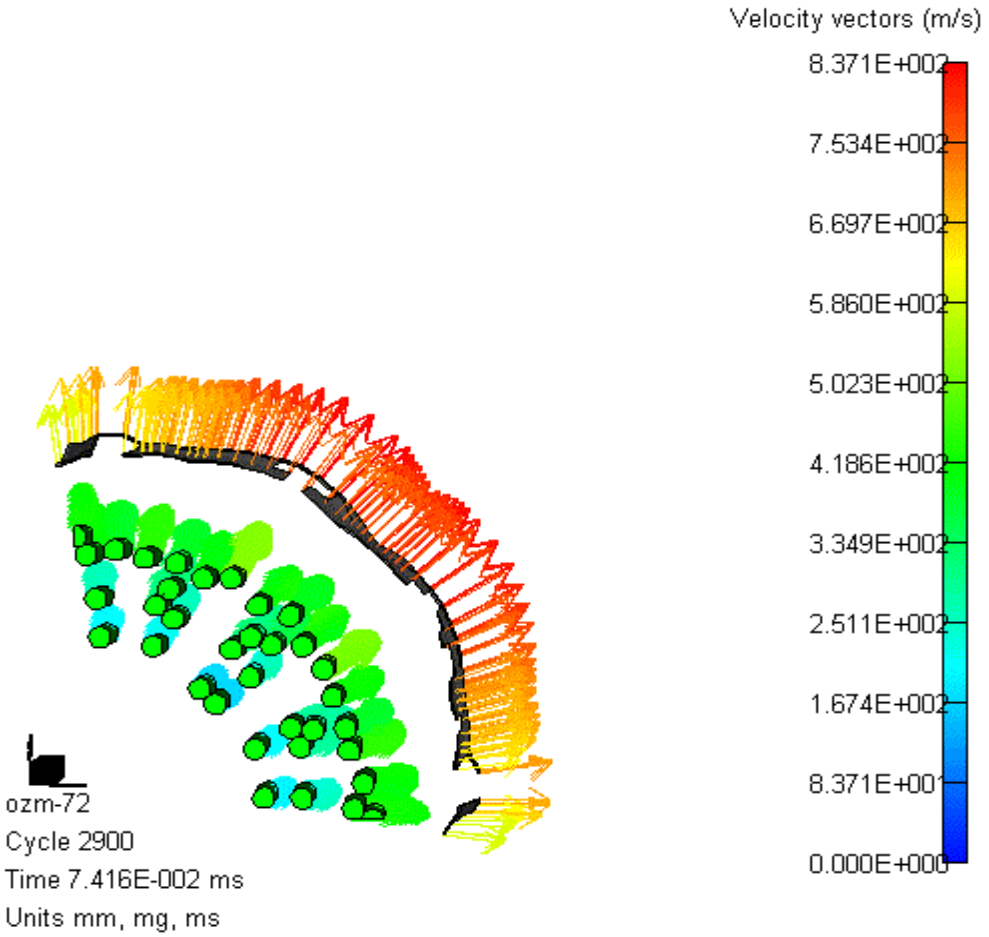

Figure 28. Four-Row Mine Model Velocities at 0.074ms

By 0.159ms (10000 cycles) the shell sub grid has significantly deformed and is in multiple pieces with the wire sub grid radially distributed in a bunched fashion. The final wire and shell configuration is shown in Figure 29 with the final velocities shown in Figure 30.

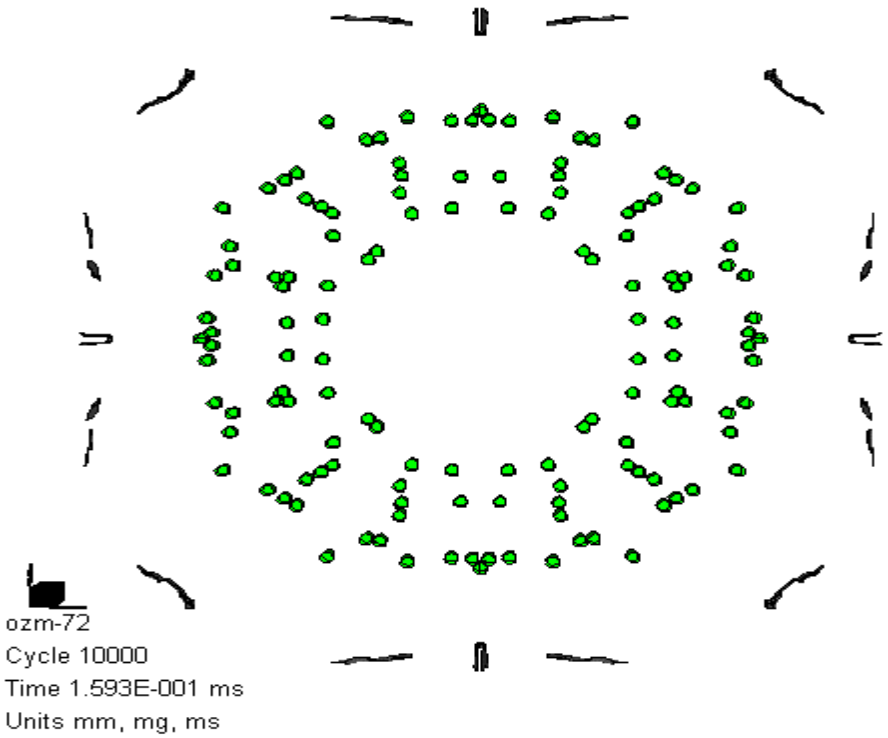

Figure 29. Expansion of the Four-Row Mine Model at 0.159ms

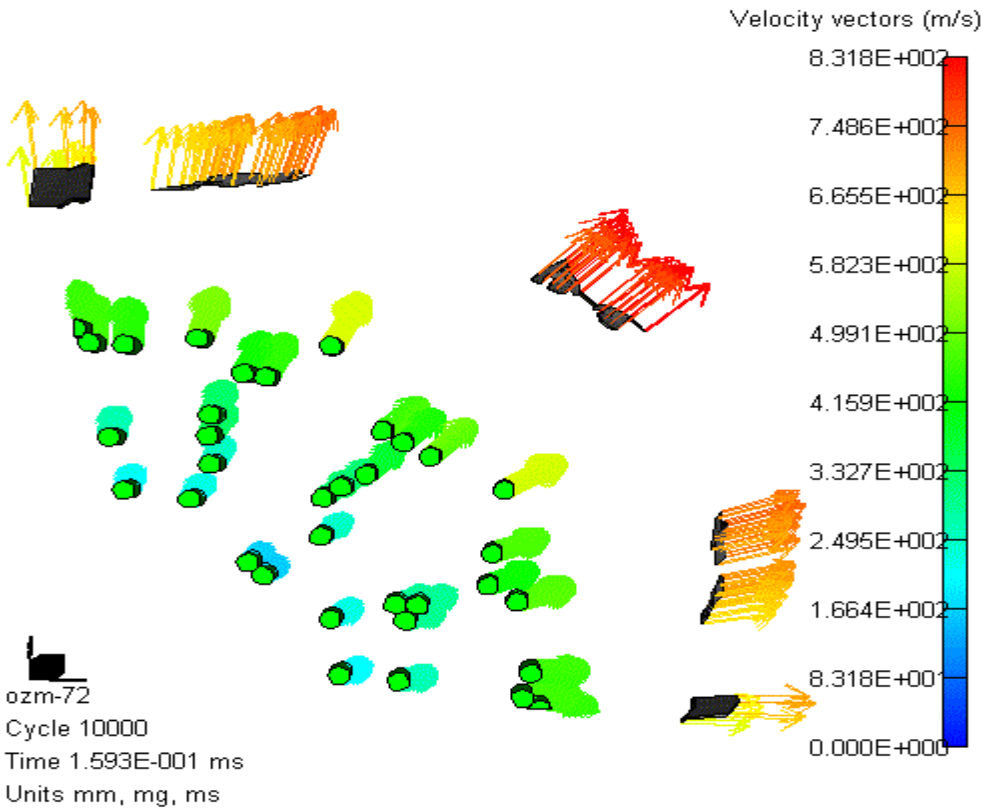

Figure 30. Four-Row Mine Model Velocities at 0.159ms

The target point locations for this model are mapped in Figure 31. At these target points time history responses were computed. The pressure applied to the targets and the absolute velocity response at targets 1, 2, 3, 4, 5 and at targets 6, 7, 8, 9 are plotted and displayed in Figure 32. The peak pressures ranged from $11x10^5$ kPa to $5x10^5$ kPa with the lower peak pressures occurring at the outer most targets. The pressure increased to the peak pressure almost instantaneously and then decayed exponentially as time increased. This is what should be expected since an explosive shock wave was used in modeling the mine explosion. The peak velocities ranged from 200 m/s to 450 m/s. The lower velocities tend to be the inner most fragments while the outer fragments had the higher velocities. The oscillation in the pressure and the velocity plots appears to have been caused by the fragments coming in contact with the symmetry boundary along the z-axis.

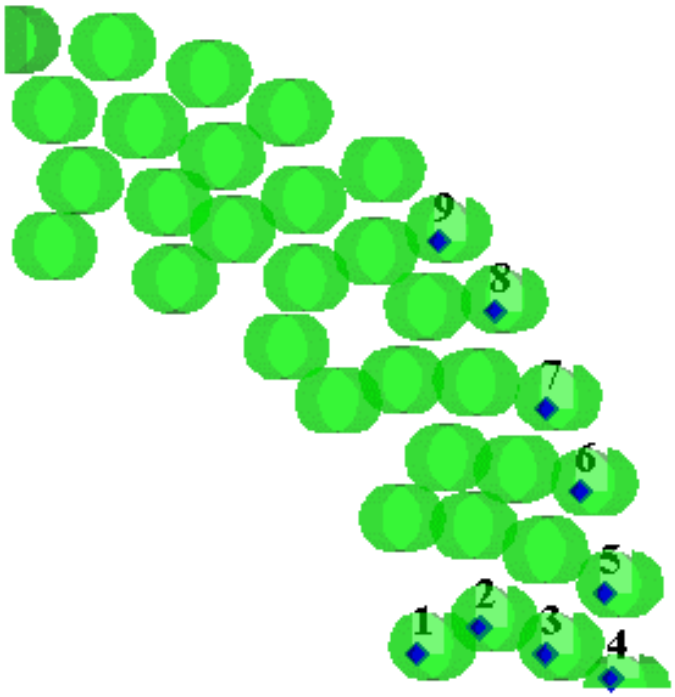

Figure 31. Four-Row Mine Model Target Point Locations

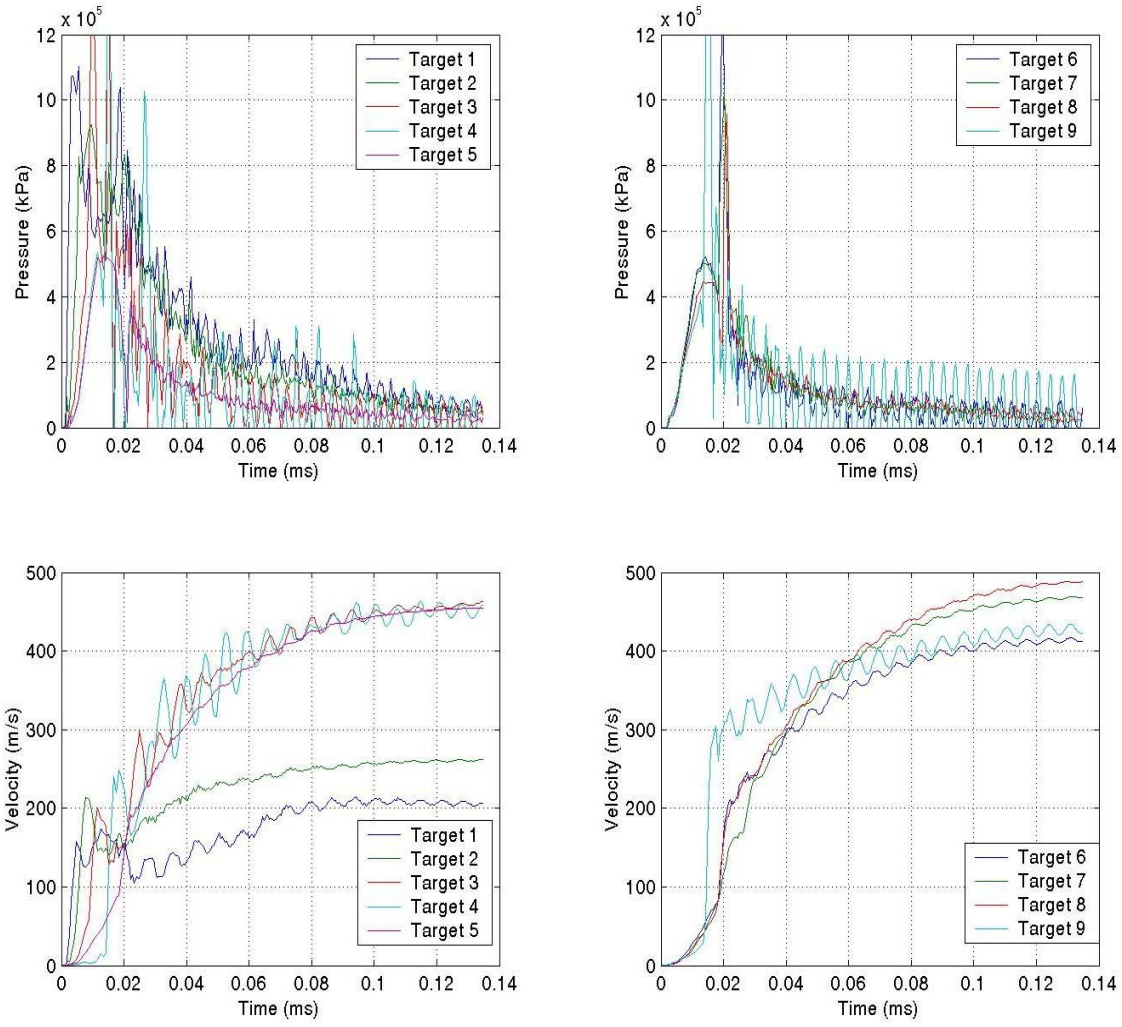

Figure 32. Four-Row Mine Model Pressure and Velocity Time History Plots

B. THREE-ROW MINE MODEL

The simulation of the three-row mine model required a run time of approximately 8 hours and 41 minutes and a total of 6000 time steps were computed, with a final cycle time of 0.201ms.

After 0.103ms (3000 cycles) the shell sub grid and the wire sub grid have expanded in the radial direction as shown in Figure 33. With Figure 34 showing the wire and shell sub grids velocities for the same cycle.

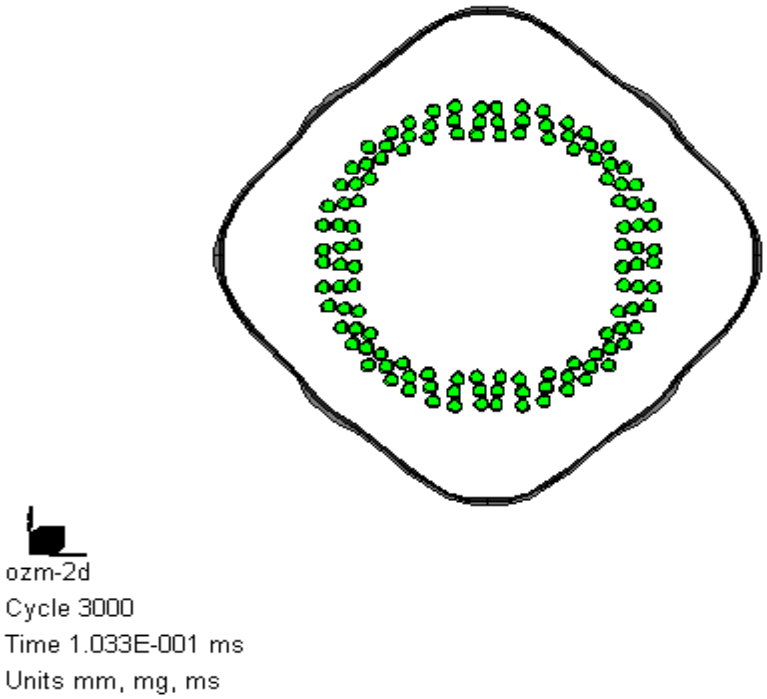

Figure 33. Expansion of the Three-Row Mine Model at 0.103ms

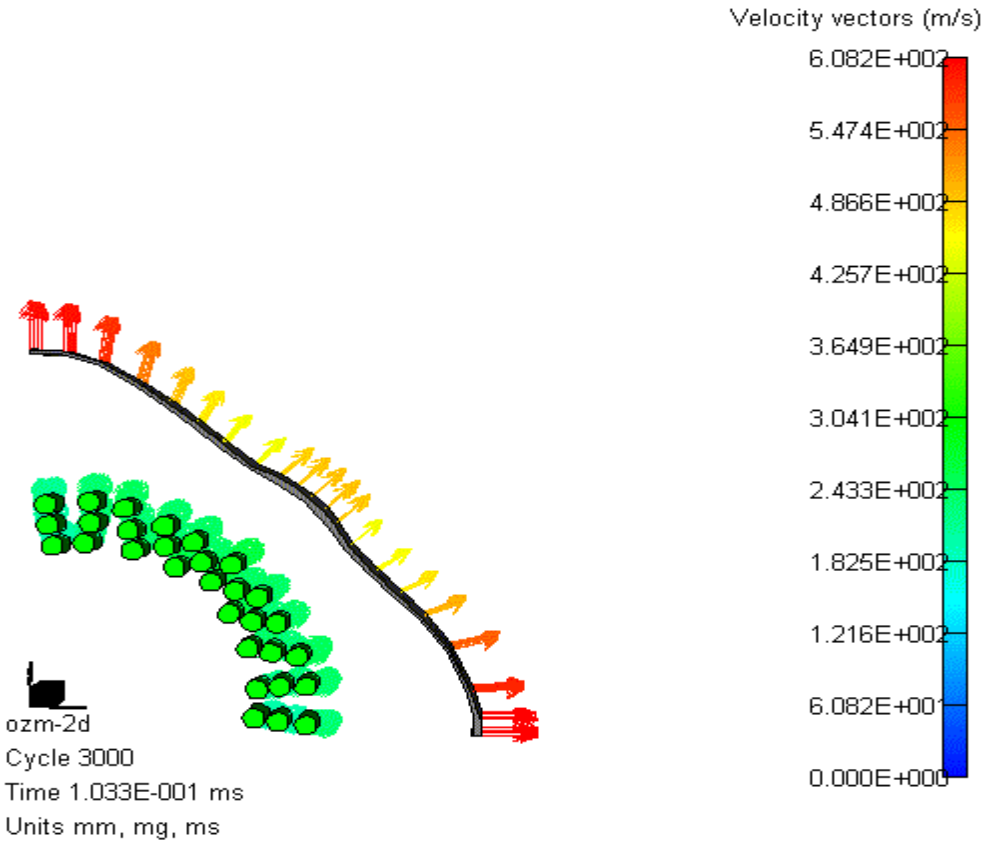

Figure 34. Three-Row Mine Model Velocities at 0.103ms

By 0.201ms (6000 cycles) the shell sub grid has started to break apart and is in several pieces. The wire sub grid is radially distributed in a fairly symmetric manner. The final wire and shell configuration is shown in Figure 35 with the final velocities shown in Figure 36.

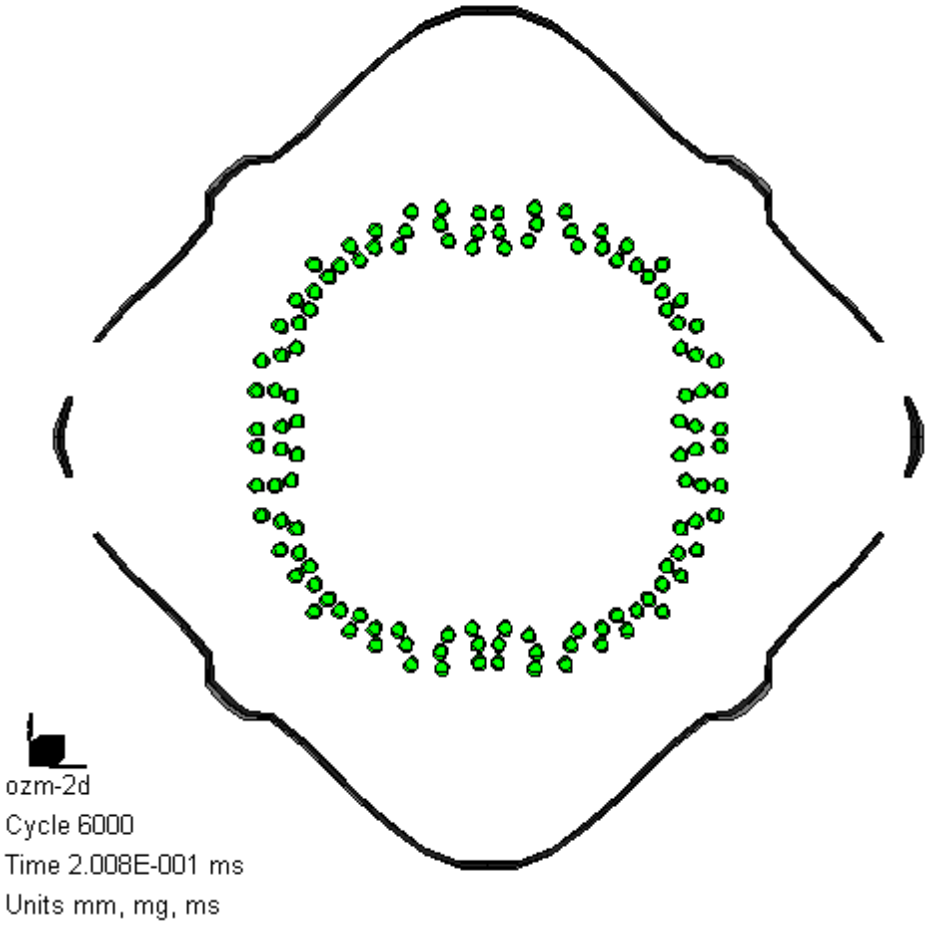

Figure 35. Expansion of the Three-Row Mine Model at 0.2ms

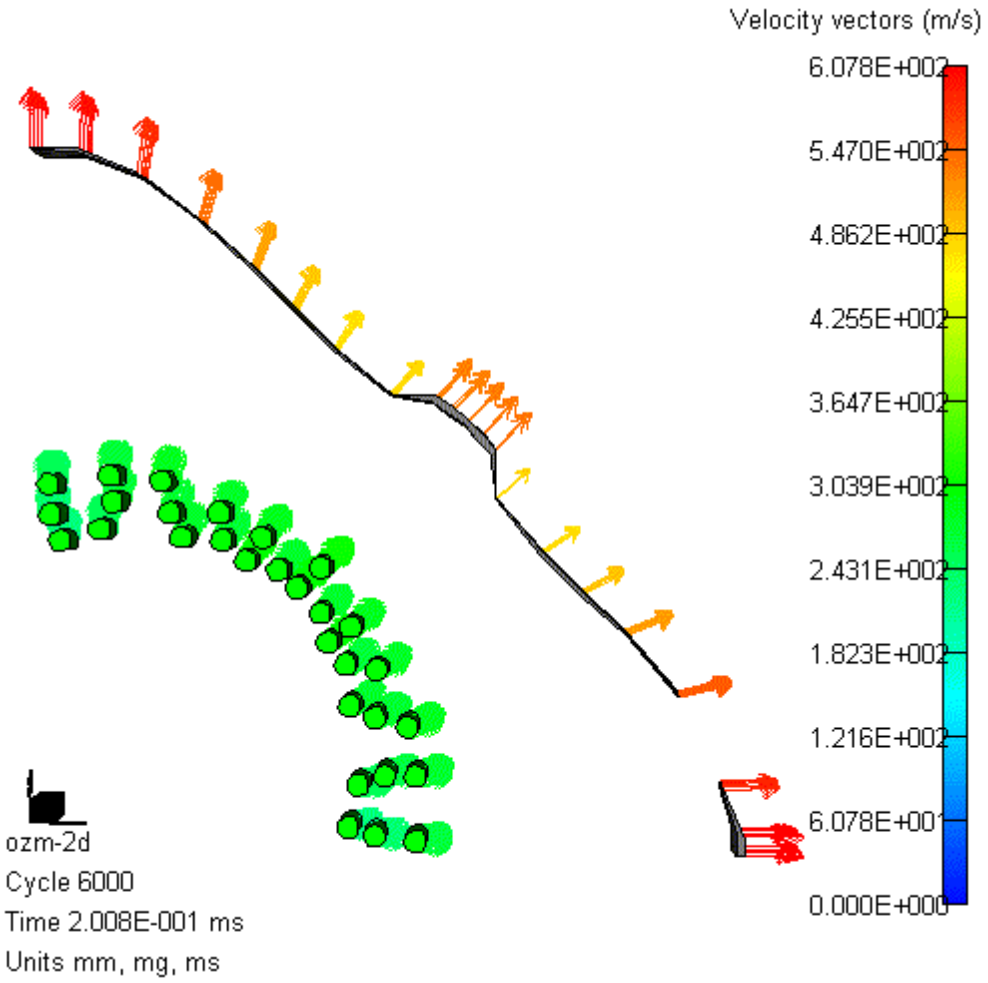

Figure 36. Three-Row Mine Model Velocities at 0.2ms

The target point locations for this model are mapped in Figure 37. At these target points time history responses are computed. The pressure applied to the targets and the absolute velocity response at targets 6, 11, 16 and at targets 8, 13, 22, 23 are plotted and displayed in Figure 38. The peak pressures ranged from $12x10^5$ kPa to $7x10^5$ kPa with the lower pressures occurring at the outer fragments. In general the pressure increases to the peak pressure almost instantaneously and then decays exponentially as time increase. This is what was expected since an explosive shock wave was used in modeling the mine explosion. The peak velocities ranged from 225 m/s to 300 m/s. The lower velocities tend to be the inner most fragments while the outer fragments have higher velocities. The sudden drops and increases in the fragments velocities seams to correspond to the

fragments hitting each other. These changes in velocity also correspond to the spikes in the pressure plots.

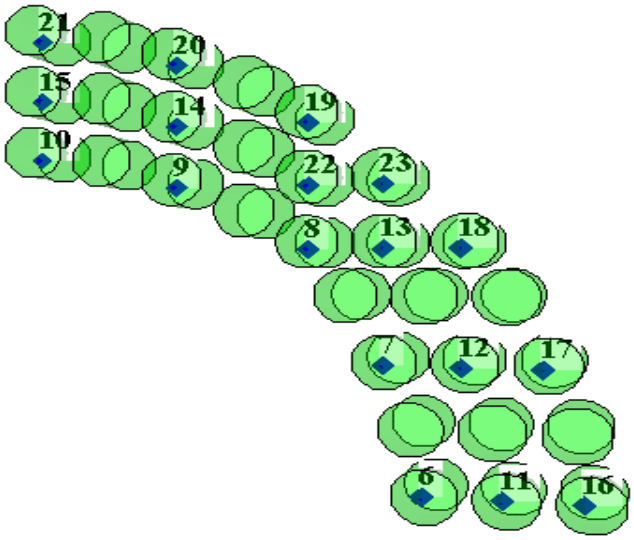

Figure 37. Three-Row Mine Model Target Point Locations

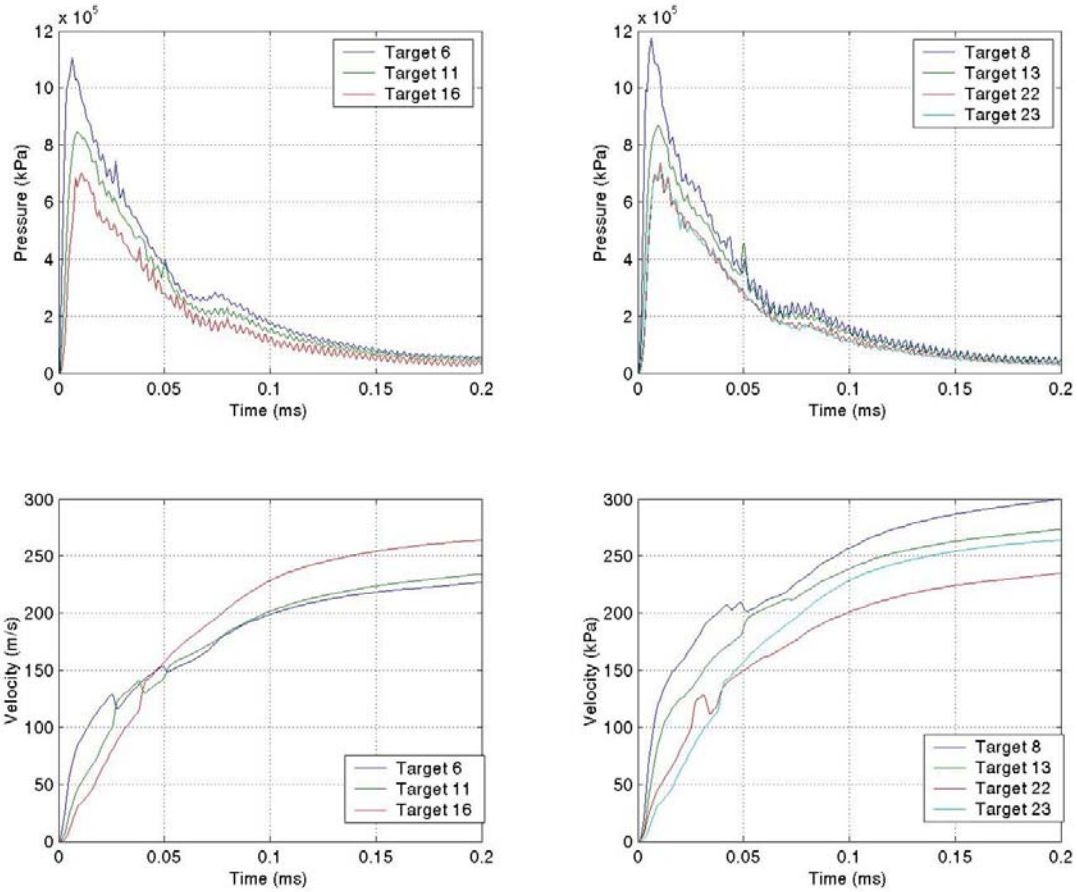

Figure 38. Three-Row Mine Model Pressure and Velocity Time History Plots

C. TWO-ROW MINE MODEL

The simulation of the two-row mine model required a run time of approximately 2 hours and 32 minutes and a total of 7000 time steps were computed, with a final cycle time of 0.216ms.

After 0.12ms (3500 cycles) the shell sub grid and the wire sub grid have expanded radially with the shell sub grid starting to break apart as shown in Figure 39 with Figure 40 showing the wire and shell sub grid velocities for the same cycle.

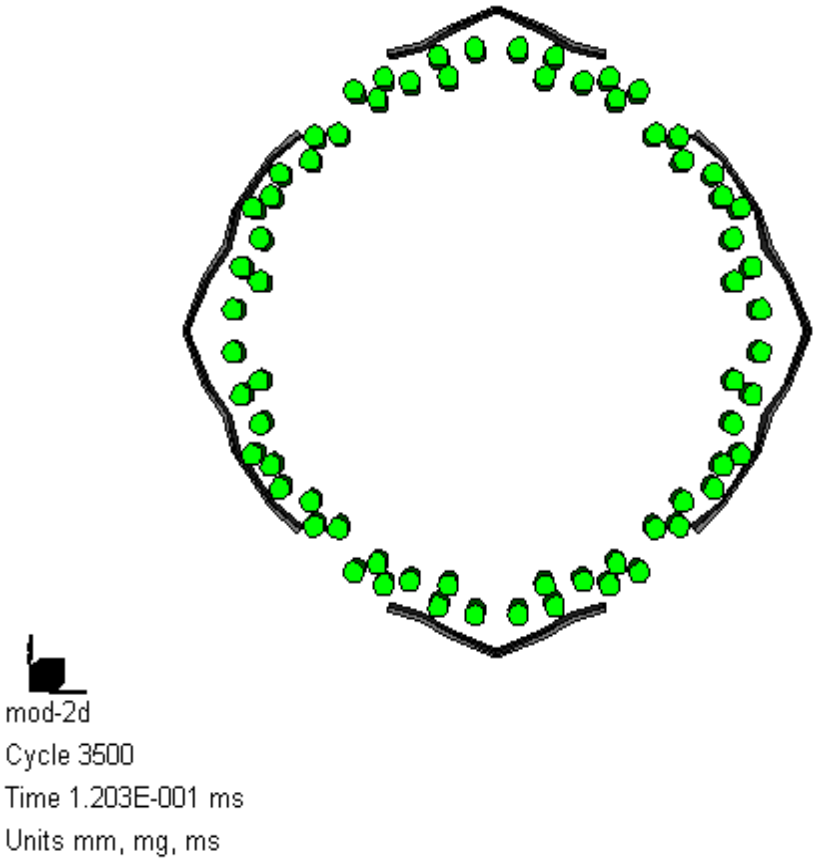

Figure 39. Expansion of the Two-Row Mine Model at 0.12ms

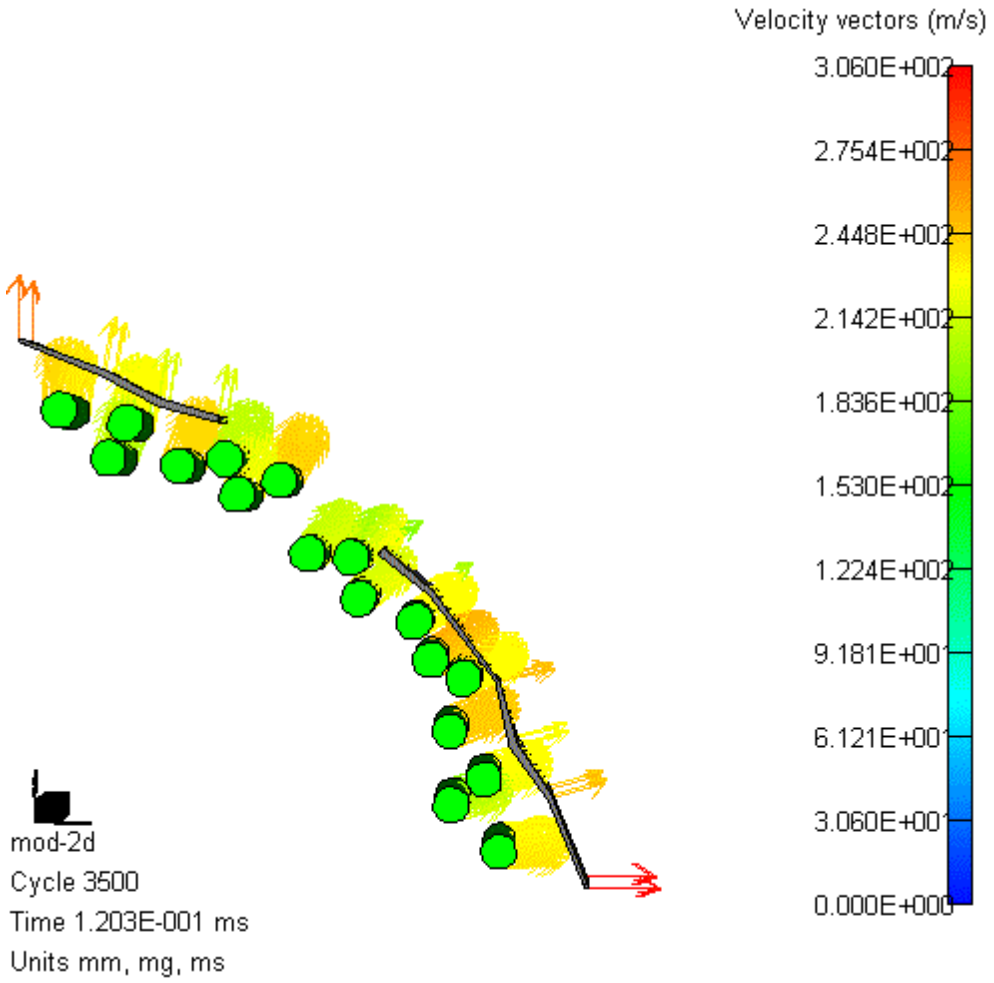

Figure 40. Two-Row Mine Model Velocities at 0.12ms

By 0.216ms (7000 cycles) the shell is completely fragmented and is intermingled with the wire fragments. The fragments are fairly evenly distributed with several small groups of fragments. The final wire and shell configuration is shown in Figure 41 with the final velocities shown in Figure 42.

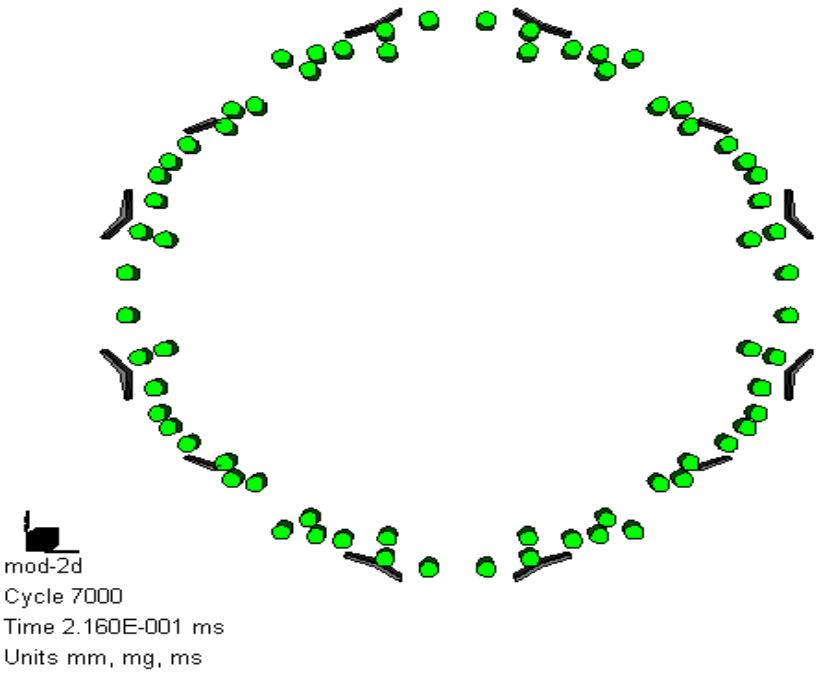

Figure 41. Expansion of the Two-Row Mine Model at 0.216ms

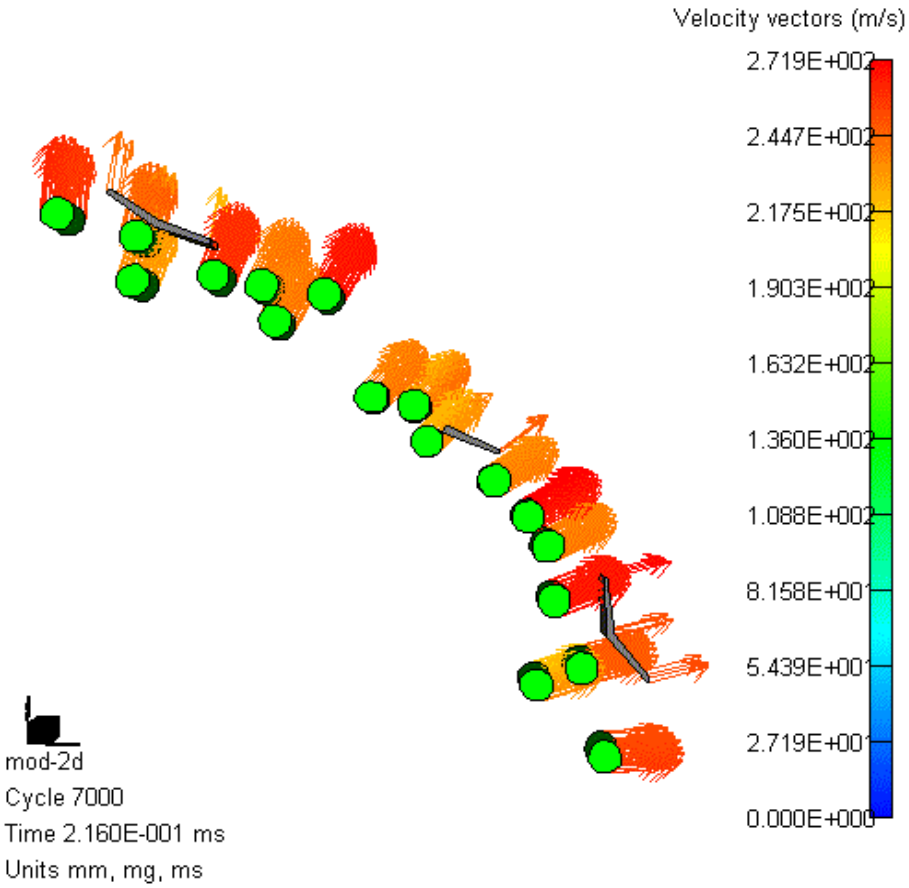

Figure 42. Two-Row Mine Model Velocities at 0.216ms

The target point locations for this model are mapped in Figure 43. At these target points time history responses are computed. The pressure applied to the targets and the absolute velocity response at targets 1, 2, 3 and at targets 8, 9, 10 are plotted and displayed in Figure 44. The peak pressure ranged from $8x10^5$ kPa to $5x10^5$ kPa. The pressure increases to the peak pressure almost instantaneously and then decays exponentially as time increase. This is what should be expected since an explosive shock wave was used in modeling the mine explosion. The peak velocities ranged from 225 m/s to 250 m/s. The velocities of the targets for this model were for the most uniform with them within 25 m/s of each other. In addition, discontinuities in the velocity and pressure plots occurred. These appear to have been caused by the fragments colliding with each other or the shell sub grid.

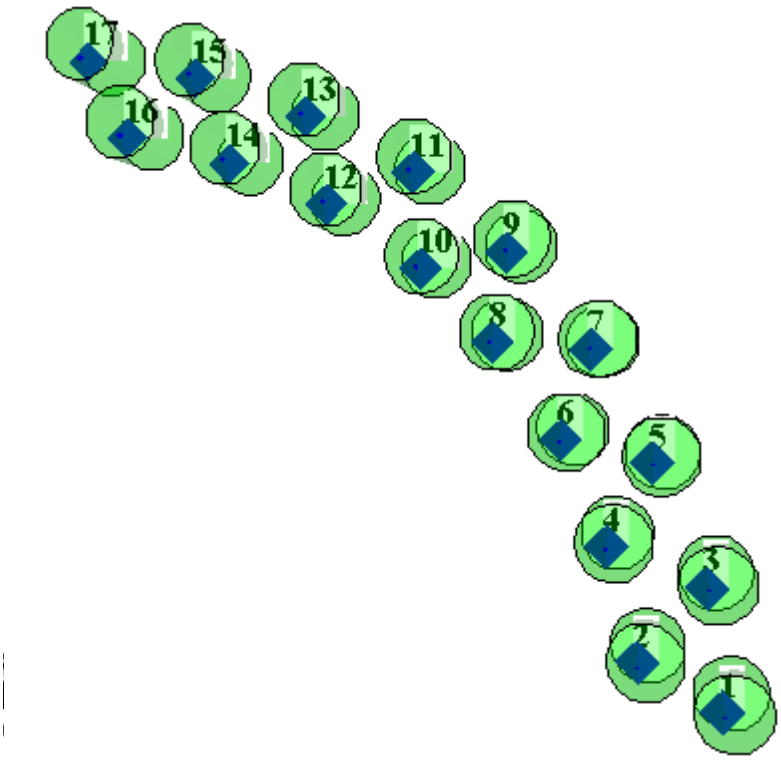

Figure 43. Two-Row Mine Model Target Point Locations

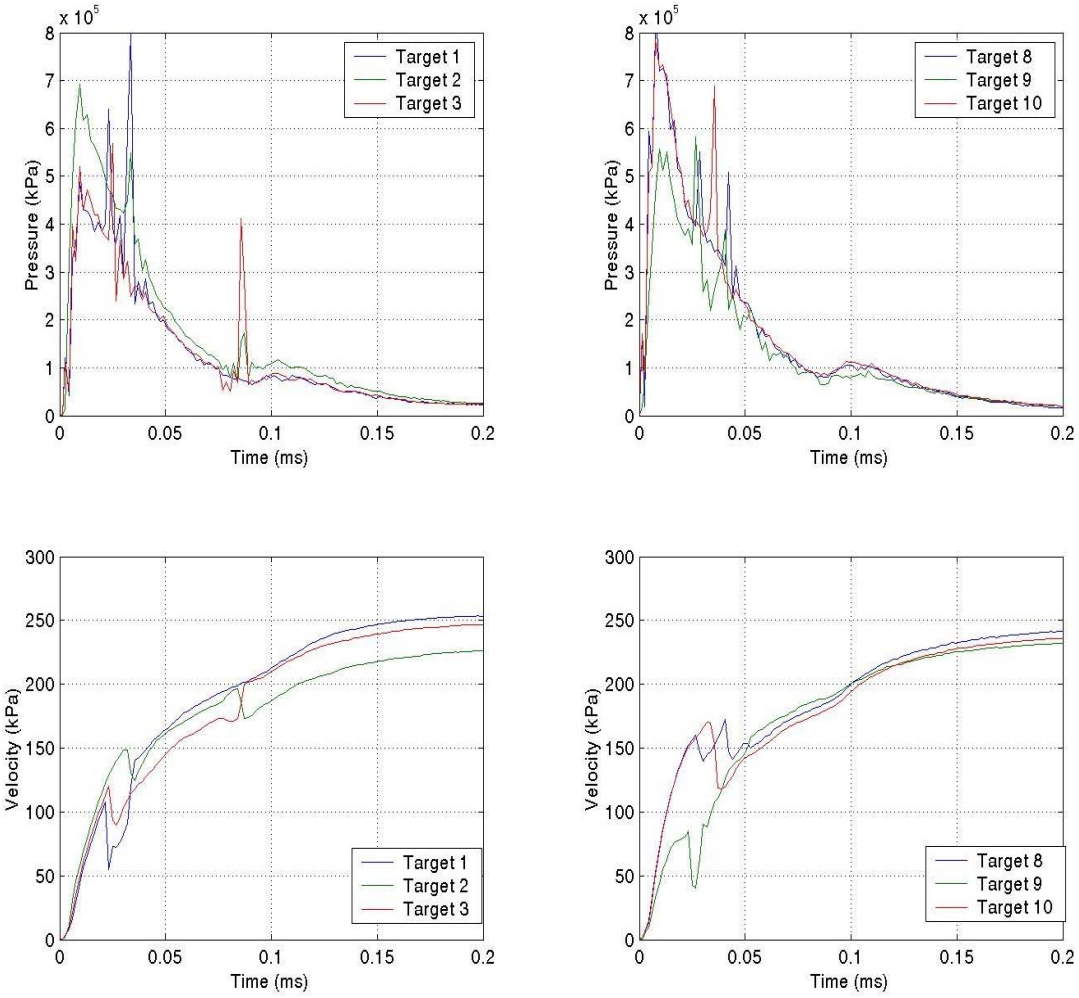

Figure 44. Two-Row Mine Model Pressure and Velocity Time History Plots

D. THREE-DIMENTIONAL MINE MODEL

The simulation of the three-dimensional mine model required a run time of approximately 89 hours and 32 minutes and a total of 4500 time steps were computed, with a final cycle time of 0.149ms.

After 0.7ms (2200 cycles) the shell sub grid and the wire sub grid have expanded radially with the cap sub grid separated from the shell sub gird as shown in Figure 45. The velocities of the wire, shell and cap sub grids for the same cycle are shown in Figure 46.

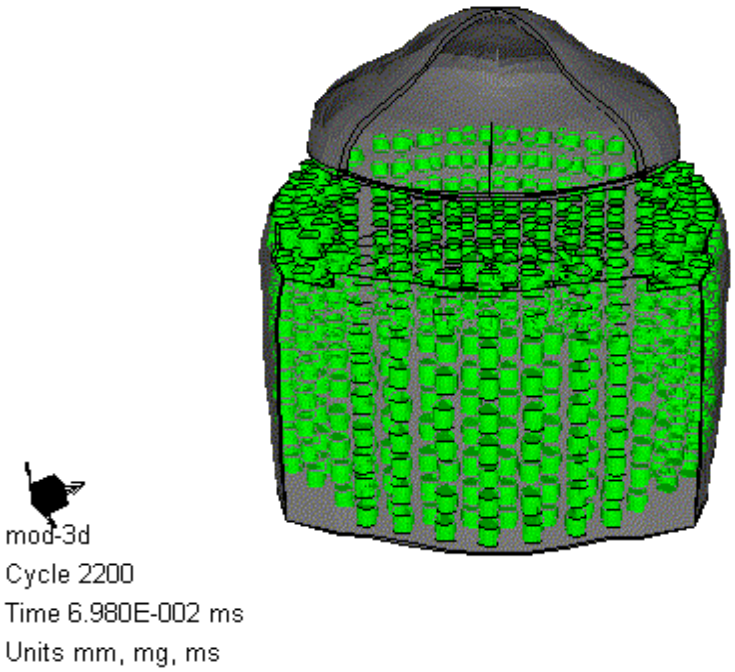

Figure 45. Expansion of the Three-Dimensional Mine Model at 0.07ms

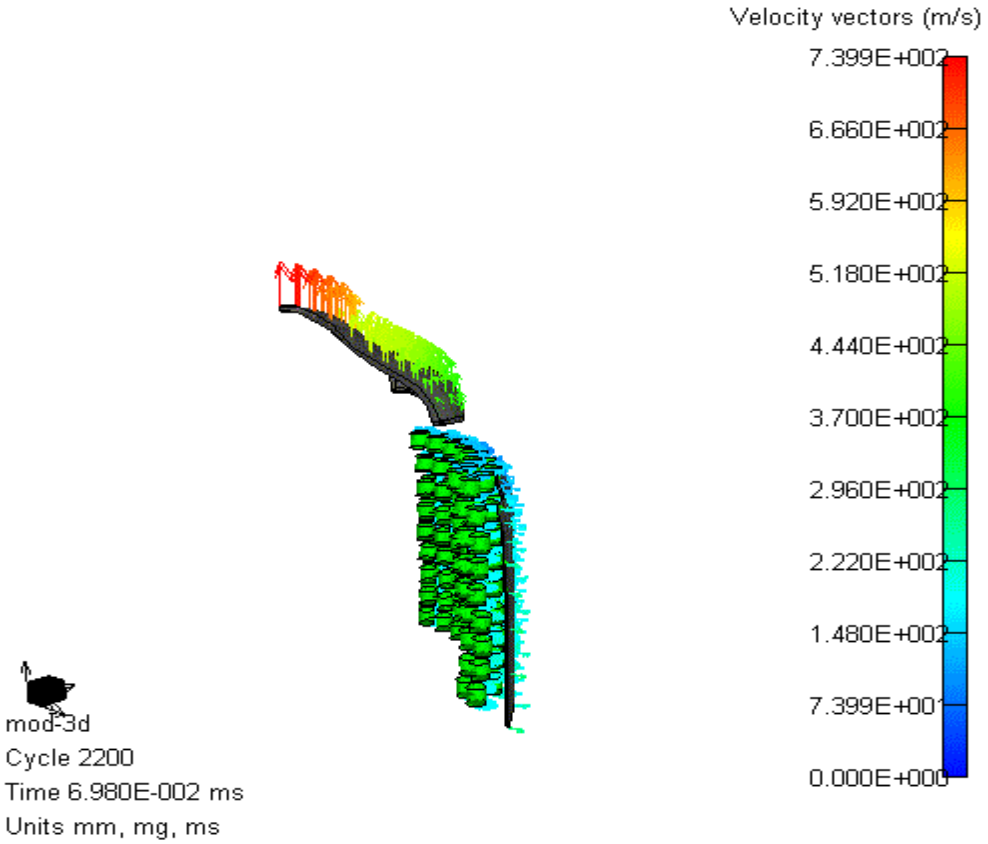

Figure 46. Three-Dimensional Mine Model Velocities at 0.07ms

By 0.149ms (45000 cycles) the shell sub grid has broken and the cap sub gird is significantly deformed. The final wire, shell and cap configurations are shown in Figure 47 with the final velocities shown in Figure 48.

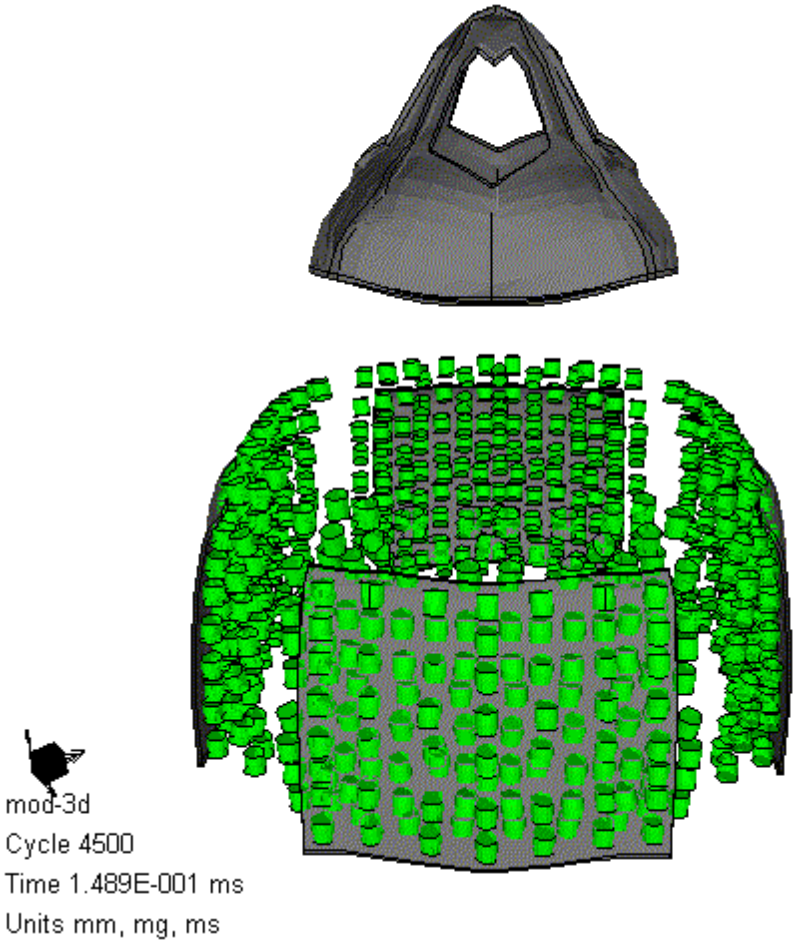

Figure 47. Expansion of the Three-Dimensional Mine Model at 0.149ms

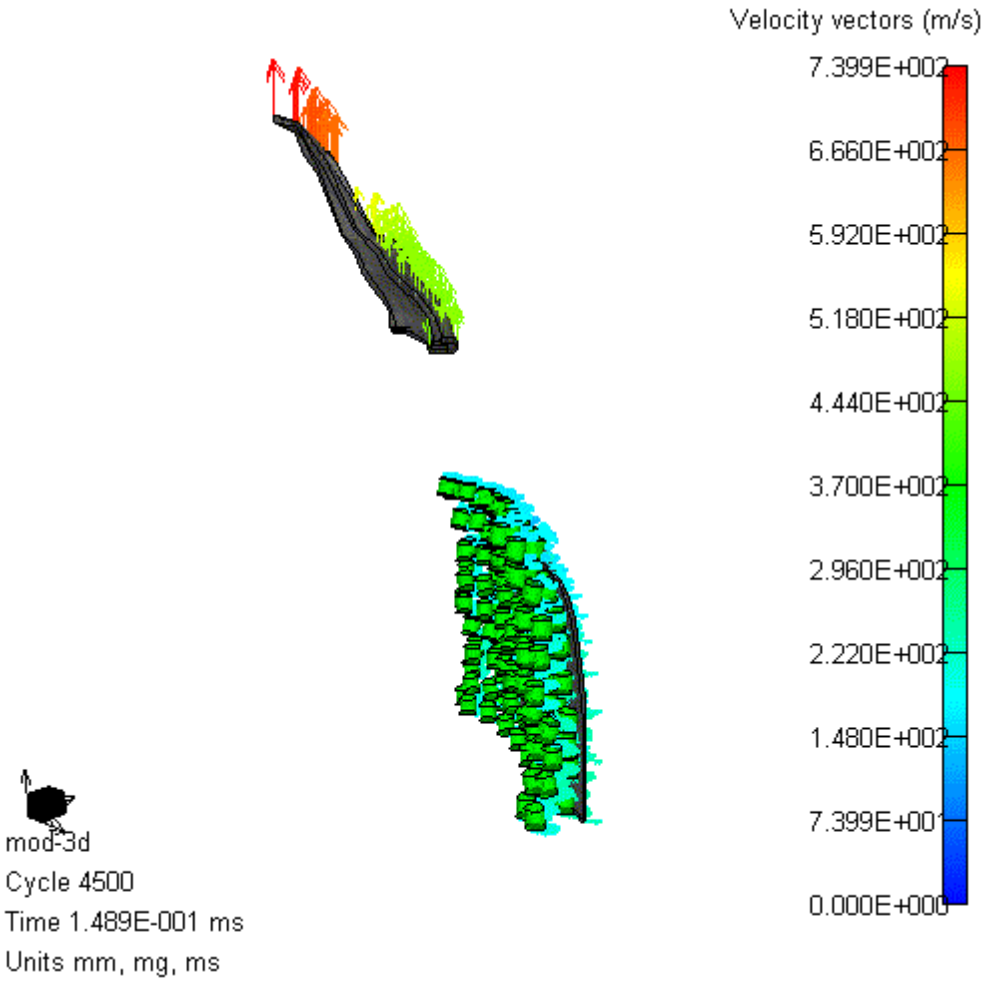

Figure 48. Three-Dimensional Mine Model Velocities at 0.149ms

The target point locations for this model are mapped in Figure 49. At these target points time history responses are computed. The pressure applied to the targets and the absolute velocity response at targets 17, 18, 19 and at targets 24, 25, 26 are plotted and displayed in Figure 50. These targets are the fragments closest to the center of the mine. The peak pressure ranged from 7.5×10^5 kPa to 5×10^5 kPa. In general these plots compare well with that of the two-row mine model. This is expected since this model was an extension of that model. The peak velocities ranged from 190 m/s to 240 m/s. The lower velocities tend to be the inner most fragments while the outer fragments have higher velocities. In general these plots compare well with that of the two-row mine model. This is expected since this model was an extension of that model.

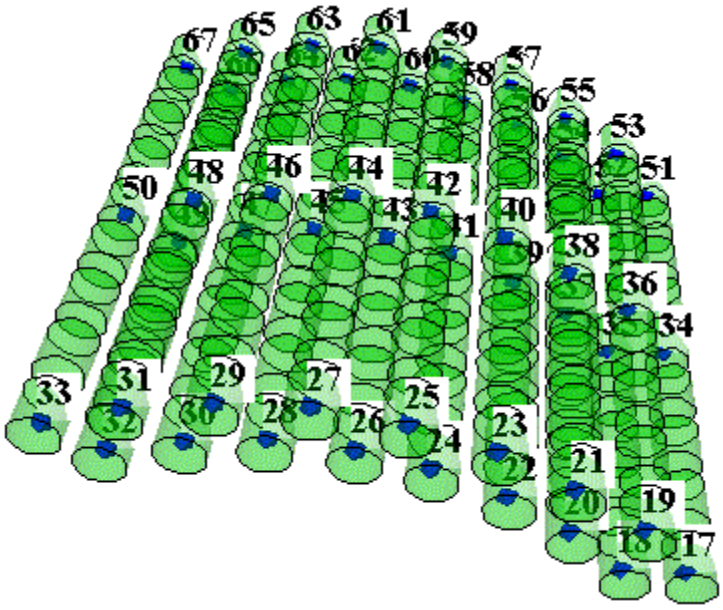

Figure 49. Three-Dimensional Mine Model Target Points

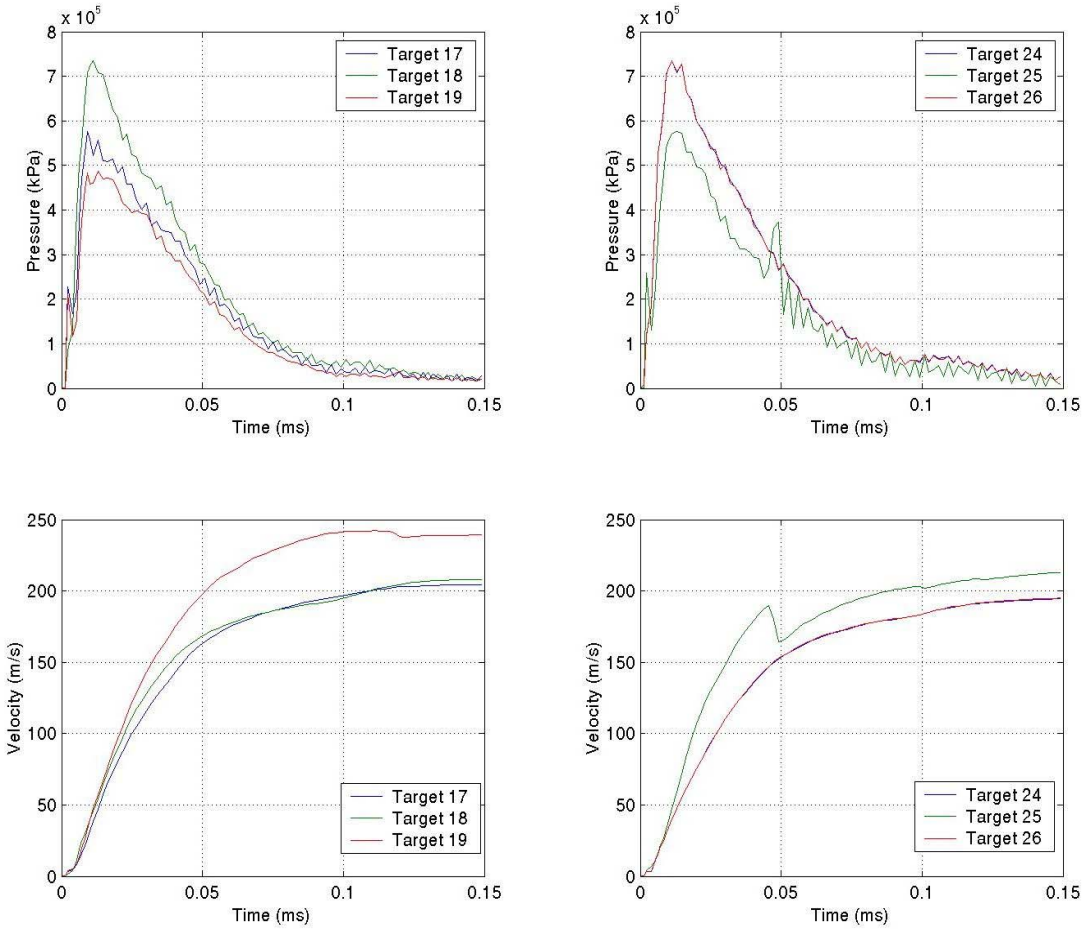

Figure 50. Three-Dimensional Mine Model Pressure and Velocity Time History Plots

The next group of target points plotted are for the targets 34, 35, 36 and 41, 42 , 43. These targets are the fragments, which are ½ of the way between the top and the middle of the mine. The peak pressure ranged from $7.5x10^5$ kPa to $4.9x10^5$ kPa with the peak velocities ranging from 175 m/s to 225 m/s. These time history plots can be found in Figure 51.

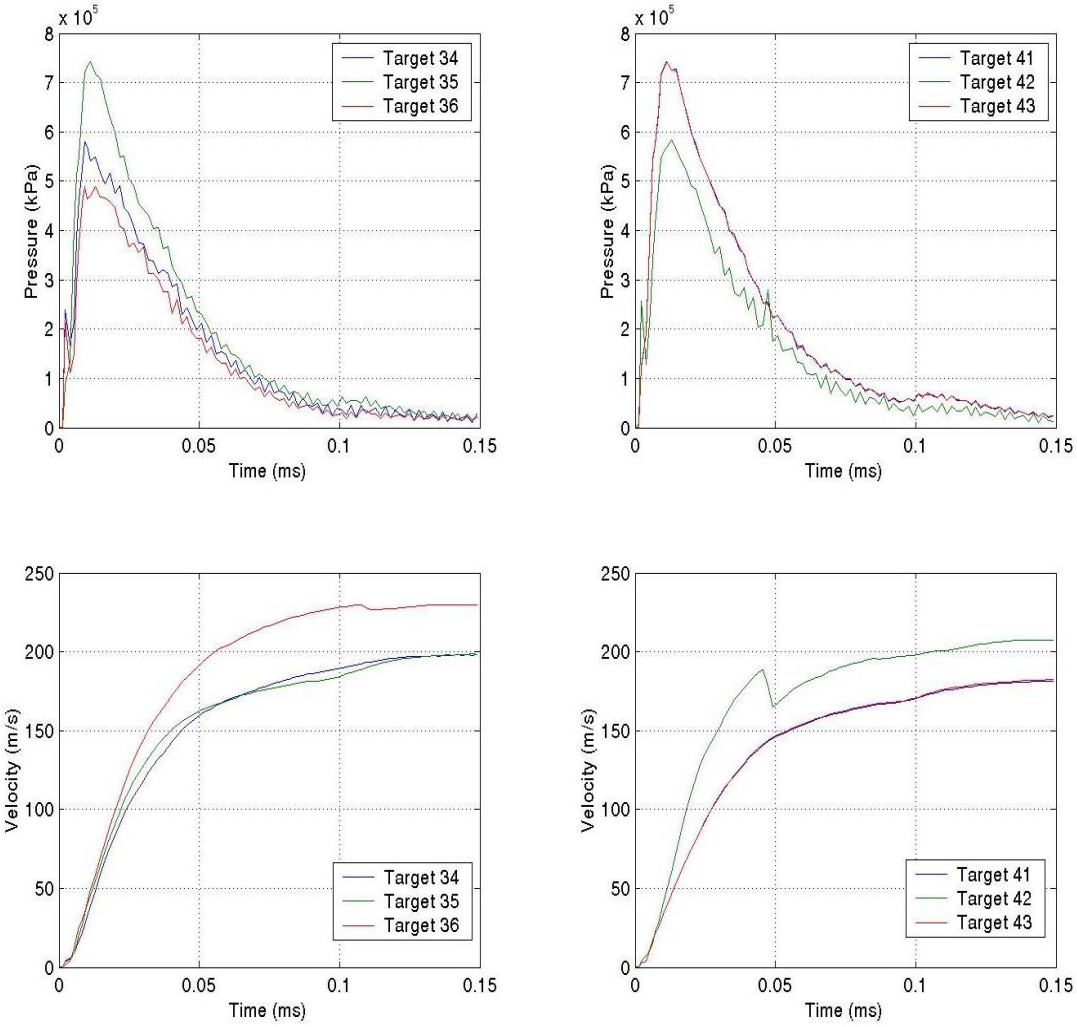

Figure 51. Three-Dimensional Mine Model Pressure and Velocity Time History Plots

The final group of target points plotted are for the targets 51, 52, 53 and 58, 59, 60. These targets are the fragments, which are at the top of the mine near the cap sub grid. The peak pressure ranged from $6x10^5$ kPa to $4x10^5$ kPa with the peak velocities ranging from 150 m/s to 175 m/s. These time history plots can be found in Figure 52.

The reason for this decrease in pressure and velocity is due to the fact that mine model is not constrained in the vertical direction. A portion of the pressure and energy is used to propel the cap sub grid upward, reducing the effect on the fragments near the cap sub grid.

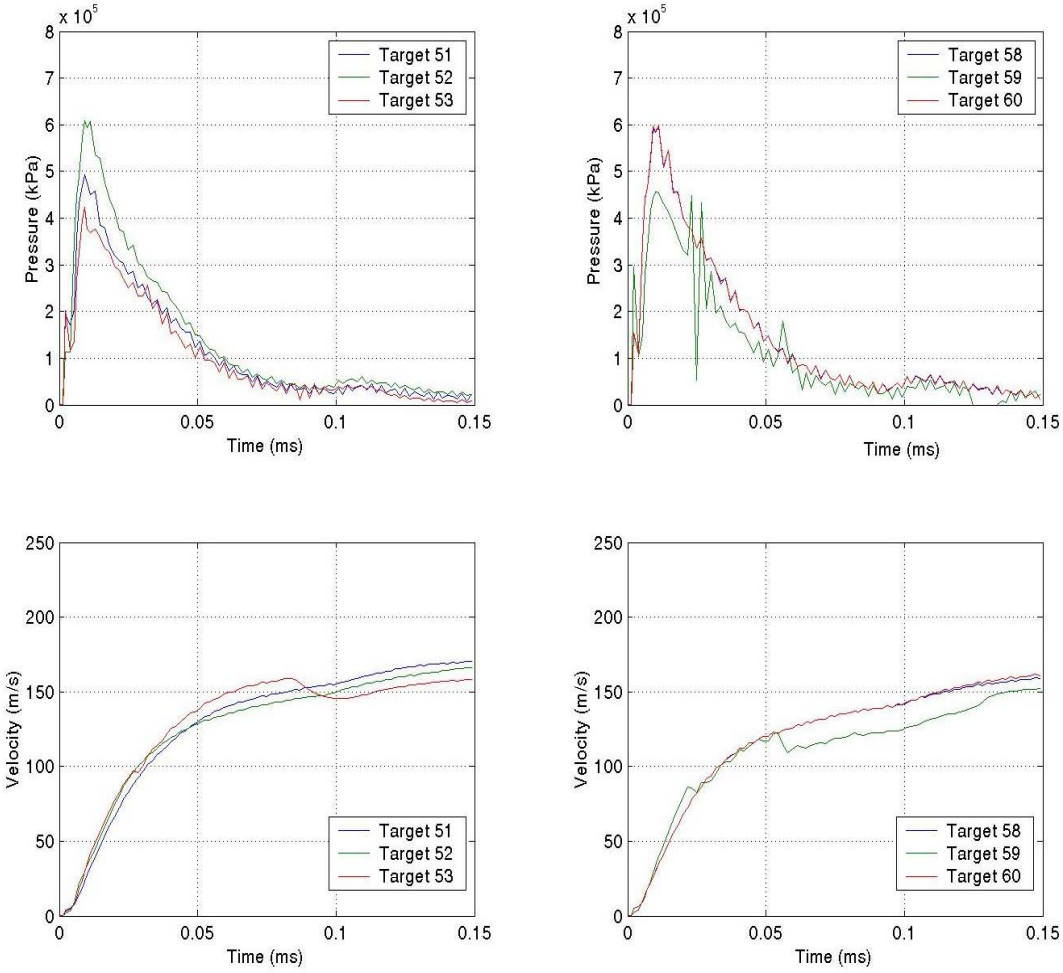

Figure 53. Three-Dimensional Mine Model Pressure and Velocity Time History Plots

An estimation of the probability of kill was computed using the three-dimensional models data to compute the results. The probability of kill was computed using the Mat Lab program provided in Appendix E. This program was developed based on the equations and assumptions outlined in Chapter III of this report. In Figure 54 the probability of kill is plotted with respect to distance for a soft target. Each line in the figure represents the targets width, which range from 0.05 m to 1 m. In Figure 55 the

same type of plot is produced for the hard target. When comparing the two plots it is apparent that for the harder target the probability of kill decays at a considerably increased rate than that of the soft target. This is due to the fact that the harder target was able to absorb more of the fragments kinetic energy.

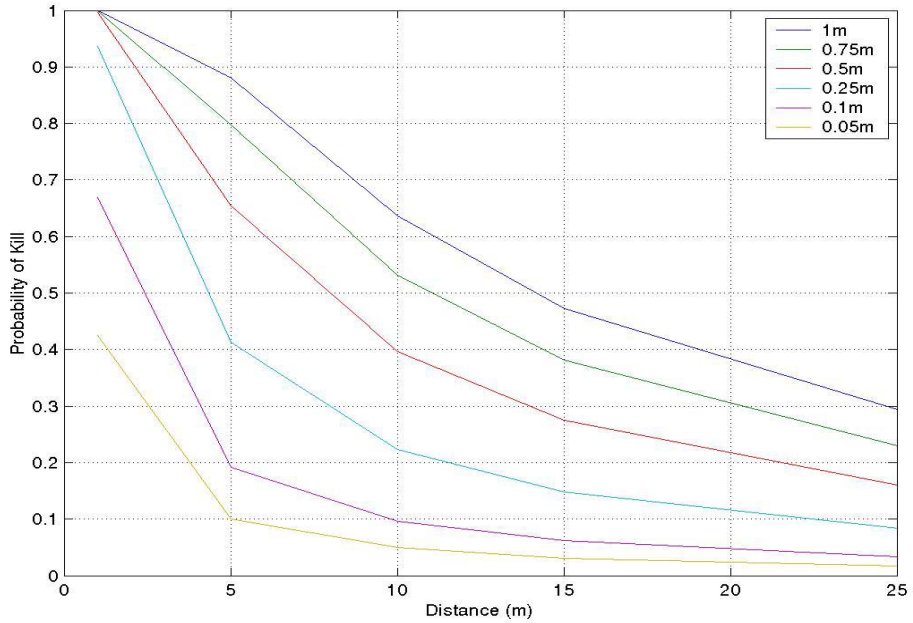

Figure 54. Estimated Probability of Kill for a Soft Target

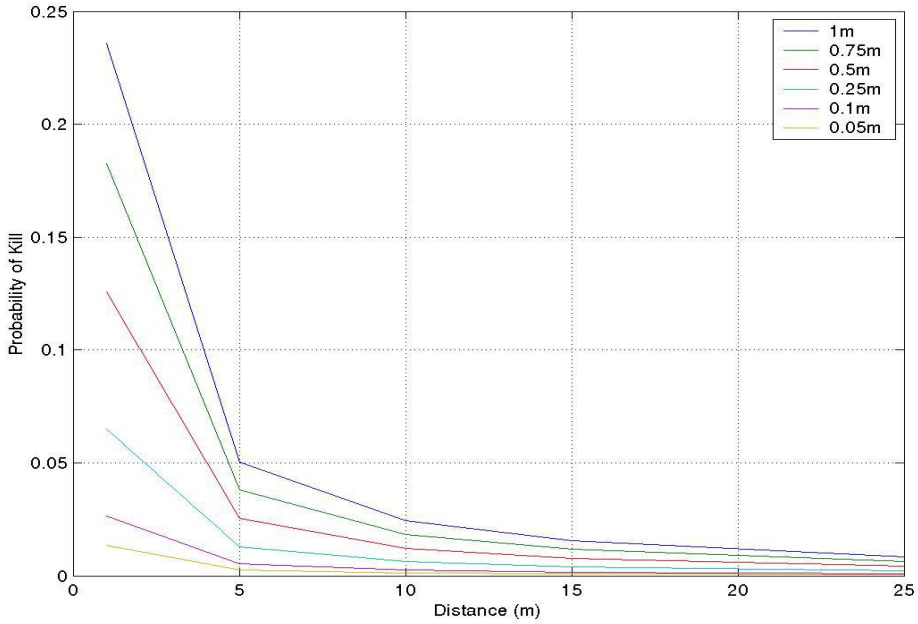

Figure 55. Estimated Probability of Kill for a Hard Target

THIS PAGE INTENTIONALLY LEFT BLANK

VI. CONCLUSIONS AND RECOMMENDATIONS

The coupled Lagrangian and Eulerian approach was used to model the detonation and fragmentation phenomena in both two and three-dimensions. The analysis results from these models demonstrated that the maximum fragment velocity is extremely high, releasing high kinetic energy. In addition the probability of kill for soft and hard targets was estimated as a function of the stand off distance. This revealed that the rate of decay of the probability of kill for the hard target was considerably faster than that of the soft target. The coupled Lagrangian and Eulerian approach may be adequate for the modeling to the fragmentation phenomena.

It is recommended that additional studies be conducted into the detonation and fragmentation phenomena. These studies include but are not limited to an investigation into what effect the resin that holds the fragments in place has on the fragmentation effect. In addition the development of equations of state and material models that take thermal effects into account could be beneficial in modeling this phenomena.

THIS PAGE INTENTIONALLY LEFT BLANK

APPENDIX A. MATIERIAL INPUT DECK FOR TNT SUB GRID

MATERIAL NAME: TNT

EQUATION OF STATE: JWL (Explosive)

Reference density (g/cm3): 1.63000E+00

Parameter C_1 (kPa): 3.73770E+08

Parameter C_2 (kPa): 3.74710E+06

Parameter R1: 4.15000E+00

Parameter R2: 9.00000E-01

Parameter W: 3.50000E-01

C-J Detonation velocity (m/s): 6.93000E+03

C-J Energy / unit volume (kJ/m3): 6.00000E+06

C-J Pressure (kPa): 2.10000E+07

Burn on compression fraction: 0.00000E+00

Pre-burn bulk modulus (kPa): 0.00000E+00

Adiabatic constant (kPa): 0.00000E+00

STRENGTH MODEL: None (Hydro)

FAILURE MODEL: None

EROSION MODEL: None

THIS PAGE INTENTIONALLY LEFT BLANK

APPENDIX B. MATERIAL INPUT DECK FOR AIR SUB GRID

MATERIAL NAME: AIR

EQUATION OF STATE: Ideal Gas

Gamma: 1.40000E+00

Reference density (g/cm3): 1.22500E-03

Adiabatic Constant (g/cm3): 0.00000E+00

Pressure shift (kPa): 0.00000E+00

Reference Temperature (K): 2.88200E+02

Specific Heat (C.V.) (J/kgK): 7.17300E+02

STRENGTH MODEL: None (Hydro)

FAILURE MODEL: None

EROSION MODEL: None

THIS PAGE INTENTIONALLY LEFT BLANK

APPENDIX C. MATERIAL INPUT DECK FOR WIRE SUB GRID

MATERIAL NAME: WIRE

EQUATION OF STATE: Linear

Reference density (g/cm3): 7.90000E+00

Bulk Modulus (kPa): 2.00000E+08

Reference Temperature (K): 0.00000E+00

Specific Heat (C.V.) (J/kgK): 0.00000E+00

STRENGTH MODEL: Elastic

Shear Modulus (kPa): 9.00000E+07

FAILURE MODEL: None

EROSION MODEL: None

THIS PAGE INTENTIONALLY LEFT BLANK

APPENDIX D. MATERIAL INPUT DECK FOR SHELL AND CAP SUB GRIDS

MATERIAL NAME: STEEL

EQUATION OF STATE: Linear

Reference density (g/cm3): 7.90000E+00

Bulk Modulus (kPa): 2.00000E+08

Reference Temperature (K): 0.00000E+00

Specific Heat (C.V.) (J/kgK): 0.00000E+00

STRENGTH MODEL: Von Mises

Shear Modulus (kPa): 9.00000E+07

Yield Stress (kPa): 2.00000E+05

FAILURE MODEL: Bulk Strain

Ultimate Strain: 1.50000E-01

Crack Softening, Gf (J/m2): 0.00000E+00

or, Kc (mN/m3/2): 0.00000E+00

EROSION MODEL: Inst. Geo. Strain

Erosion Strain: 2.00000E+00

THIS PAGE INTENTIONALLY LEFT BLANK

APPENDIX E. PROBABILITY OF KILL PROGRAM

The following program was developed to estimate the probability of kill for the mine models developed in this study. The program uses the equations and assumptions outlined in Chapter III of this report.

```
load fragdata

% Constants
rho = 1.2;                      % Air Density at Standard Conditions
Cd = 2.1;                       % Drag Coefficient of a Square Cylinder
A = 0.000025;                   % Cross-Sectional Area of a Fragment
m = 0.0031;                     % Mass of a Fragment
S = [1, 5, 10, 15, 25];         % Distance from Mine
N = [1224];                     % Number of Fragments in 3D Mine Model
TA = [1, .75, .5, .25, .1, .05]; % Width of Target

% Determine the average initial velocity of the fragments.
Vor3d = mean(R3D2VEL(91,:));

% Determine the velocity of fragments at specified distances considering drag.
for n = 1:5
   Vsr3d(n,:) = Vor3d .* exp(-(rho * A * S(n))/(2 * m));        % Equation 3.2
   FragD(n) = N/(2 * pi * S(n));
end

% Determine kinetic energy of projectiles based on velocity at specified distances.
KEr3d = (Vsr3d.^2) .* (1/2) * m;                                % Equation 3.1

% Determine Probability of  Kill for Targets
Pkh1 = (KEr3d ./ 100) .* 0.1;                                   % Soft Target
Pkh2 = (KEr3d ./ 4000) .* 0.1;                                  % Hard Target
for i = 1:5
   for j = 1:6
      Nd(j,i) = FragD(i) * TA(j);               % Equation 3.5
      if Nd(j,i) > 1
         PK1(j,i) = 1 -(1-Pkh1(i))^Nd(j,i);     % Equation 3.3
         PK2(j,i) = 1 -(1-Pkh2(i))^Nd(j,i);
      else
         PK1(j,i) = Nd(j,i) * Pkh1(i);          % Equation 3.4
         PK2(j,i) = Nd(j,i) * Pkh2(i);
      end
   end
end
figure (1)
plot(S',PK1)
legend ('1m','0.75m','0.5m','0.25m','0.1m','0.05m')
figure (2)
plot(S',PK2)
legend ('1m','0.75m','0.5m','0.25m','0.1m','0.05m')
```

THIS PAGE INTENTIONALLY LEFT BLANK

LIST OF REFRENCES

1. Kinney, G.F. and Graham, K.J., Explosive Shocks in Air, 2d ed., Springer-Verlag New York Inc., 1985.

2. Ball, R.B., The Fundamentals of Aircraft Combat Survivability Analysis and Design, pp. 188-190, American Institute of Aeronautics and Astronautics, Inc., 1985.

3. Century Dynamics, AUTODYN Users Manuel, Revision 3.0, Century Dynamics Inc., 1997.

4. Century Dynamics, AUTODYN Theory Manuel, Revision 4.0, Century Dynamics Inc., 1998.

5. "MINES AND BOOBY TRAPS CURRENTLY DEPLOYED, RUSSIAN FEDERATION AND ASSOCIATED STATES (CIS)" [http://onlines.janes.com] October 2000.

6. "OZM-72" [http://www.Angola.npaid.org/mine_Russia_ozm_72.htm]. October 2000.

7. Century Dynamics, AUTODYN Introductory Training Course, Century Dynamics Inc., January 2001.

8. United Defense, "Grizzly" [http://www.uniteddefense.com/markets/defense/combat/support/vehicle/index.htm]. October 2000.

9. Zukas, J.A., and others, Impact Dynamics, John Wiley & Sons Inc., 1982.

10. Zukas, J.A., High Velocity Impact Dynamics, John Wiley & Sons Inc., 1990.

11. United States Naval Academy, Introductions to Naval Weapons Engineering [http://131.122.80/wse/academic/courses/es310/]. January 2000.

12. FAS Military Analysis Network, "Grizzly [Breach]" [http://www.fas.org/man/dod-101/sys/land/grizzly.htm]. May 2000.

THIS PAGE INTENTIONALLY LEFT BLANK

INITIAL DISTRIBUTION LIST

1. Defense Technical Information Center
   Fort Belvoir, Virginia

2. Dudley Knox Library
   Naval Postgraduate School
   Monterey, California

3. Professor Young Shin
   Naval Postgraduate School
   Monterey, California

4. COL Michael K. Asada
   Combat Mobility Systems
   AMSTA-LC-AC
   Warren, Michigan

5. Mr. Brian Bonkosky
   U.S. Army TACOM
   AMSTA-LC-AC-G (415)
   Warren, Michigan

6. Mr. Darrol Spurgeon
   U.S. Army TACOM
   AMSTA-LC-AC-G (415)
   Warren, Michigan